arXiv:1311.1726v2 [q-bio.BM] 27 Nov 2013

Internal water and microsecond dynamics in myoglobin

Shuji Kaieda and Bertil Halle

Department of Biophysical Chemistry, Lund University, Lund, Sweden

Myoglobin (Mb) binds diatomic ligands, like O_2, CO, and NO, in a cavity that is only transiently accessible. Crystallography and molecular simulations show that the ligands can migrate through an extensive network of transiently connected cavities, but disagree on the locations and occupancy of internal hydration sites. Here, we use water ^{2}H and ^{17}O magnetic relaxation dispersion (MRD) to characterize the internal water molecules in Mb under physiological conditions. We find that equine carbonmonoxy Mb contains 4.5 ± 1.0 ordered internal water molecules with a mean survival time of 5.6 ± 0.5 μs at 25 °C. The likely location of these water molecules are the four polar hydration sites, including one of the xenon-binding cavities, that are fully occupied in all high-resolution crystal structures of equine Mb. The finding that water escapes from these sites, located 17 – 31 Å apart in the protein, on the same μs time scale suggests a global exchange mechanism. We propose that this mechanism involves transient penetration of the protein by H-bonded water chains. Such a mechanism could play a functional role by eliminating trapped ligands. In addition, the MRD results indicate that two or three of the 11 histidine residues of equine Mb undergo intramolecular hydrogen exchange on a μs time scale.

1. Introduction

The 153-residue hemoprotein myoglobin (Mb) transports O_2 from sarcolemma to mitochondria in cardiac and skeletal muscle tissue of most mammals.[1] In addition to O_2, other diatomic ligands, such as CO and NO, bind to the heme iron and it has been suggested that Mb also acts as a NO scavenger.[2] Crystal structures[3–9] of Mb do not reveal the pathway(s) for ligand migration from the exterior to the buried binding site in the distal pocket (DP) at the heme-bound iron (Fig. 1). Ligand access to the heme is therefore thought to be controlled by structural fluctuations.

Despite a large amount of experimental and computational work,[10–51] the mechanism of conformationally gated ligand migration through Mb has not been firmly established. In particular, while there is wide support for the direct pathway linking the DP to the exterior via the histidine (His-64) gate, the importance of ligand migration through the network of cavities in Mb, including the four Xe binding sites (Xe1 – Xe4)[52] and the phantom (Ph) region (Fig. 1), is still debated. Furthermore, the complex kinetics of ligand migration and escape under physiological conditions have not been fully elucidated, although the relevant time scale appears to be 0.1 – 10 μs at ambient temperature.

The permanent cavities in Mb, with a combined (probe-size dependent[53]) volume approaching 300 Å^3, could accommodate a dozen water molecules, but since most of them are lined by nonpolar side-chains one expects a low water occupancy.[54,55] Indeed, high-resolution crystal structures of Mb have identified only four (equine Mb)[4,7,9] or five (sperm whale Mb)[5,6,8] internal water molecules outside the DP. The carbonmonoxy form[5–7] of Mb (MbCO) has no water in the DP, but a water molecule is found in the DP in the deoxy form[9] and is bound to the iron atom in the met form.[4–6,8] While ligand migration in Mb has been extensively studied, only a few studies have examined the involvement of internal water molecules in the mechanism and then the focus has been on the DP water.[17,30,34,41]

Information about internal water outside the DP has come from molecular dynamics (MD) simulations[44,51] and from magnetic relaxation dispersion (MRD) experiments.[56–58] The MD studies indicated several partly occupied internal hydration sites,[44,51] only some of which coincide with the crystallographic sites, but these simulations did not access the μs time scale of water and ligand migration.

The water MRD technique measures the magnetic field (or resonance frequency) dependence of the longitudinal spin relaxation rate R_1 of one of the magnetic water nuclides (^{1}H, ^{2}H, or ^{17}O).[59,60] Two of the MRD studies[56,57] employed the ^{1}H nuclide to determine the paramagnetic relaxation enhancement for the DP water in met-Mb. The more recent MRD study,[58] which used the ^{2}H and ^{17}O nuclides, concluded that equine MbCO contains at least three internal water molecules with survival times exceeding the ~ 10 ns tumbling time of Mb.

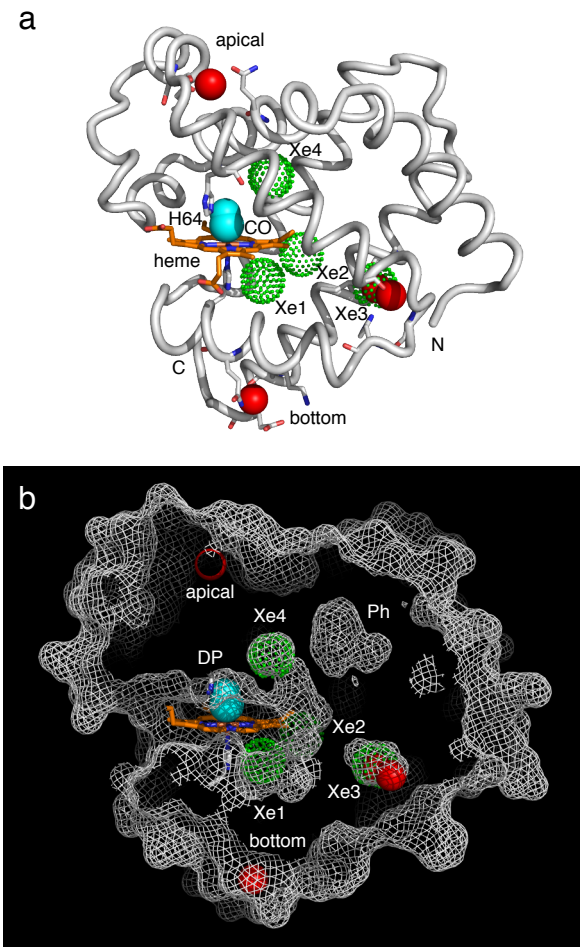


Figure 1. Crystal structure[7] 1DWR of equine MbCO in (**a**) ribbon and (**b**) cross-sectional surface (1.4 Å probe) representations, rendered with PyMol (Schrödinger, LLC). Color code: heme (orange), CO (cyan), internal water molecules (red), and xenon binding sites[52] (green).

From MRD measurements on protein solutions one can obtain the number of water molecules with survival time longer than a lower bound set by the protein tumbling time ($\sim$ 10 ns for Mb) and shorter than an upper bound set by the intrinsic spin relaxation rate for the internal water molecule ($\sim$ 1 µs for ^{17}O and $\sim$ 100 µs for ^{2}H).[59,60] But within this rather wide range, solution MRD experiments cannot differentiate water molecules with different survival times.

More information can be obtained if the protein is immobilized by a chemical cross-linking reagent such as glutaraldehyde (GA) so that molecular tumbling is inhibited. The MRD profile is then essentially the Fourier transform of the survival correlation function and survival times up to $\sim$ 10 µs of individual internal water molecules can be determined directly from the ^{2}H MRD profile.[61,62]

Here, we report an extensive set of ^{2}H and ^{17}O MRD data from equine MbCO. Water dynamics on the ns – µs time scale is characterized in detail by examining solutions with free-tumbling Mb as well as cross-linked gels with immobilized Mb, in both cases under fully hydrated conditions ($\sim$ 1.6 mM Mb). To extract quantitative information about internal water molecules from ^{2}H MRD data, it is necessary to isolate any contribution from rapidly exchanging labile deuterons in the protein. By analyzing the pD dependence of the ^{2}H MRD and by comparing with the ^{17}O MRD, we find that several histidine sidechains in Mb exchange deuterons with water on the µs time scale, apparently by an intramolecular catalytic mechanism involving an adjacent deuteron exchange catalyst, such as a carboxylate.

The principal questions that we address here are: (1) How many internal water molecules occupy the internal cavities of Mb under physiological conditions? (2) Where are they located? In particular, are the Xe binding sites hydrated? (3) How long do the internal water molecules remain inside the cavity network? (4) By what mechanism do the internal water molecules exchange? (5) Does the internal water play a purely structural role or are they involved more directly in the function of Mb?

2. Materials and methods

2.1. Sample preparation

Lyophilized equine skeletal muscle Mb was purchased from Sigma ($\geq$ 95 %) and further purified by cation-exchange chromatography (SP sepharose; GE Healthcare). The purified Mb was lyophilized following extensive dialysis against MilliQ water. To prepare carbonmonoxy Mb (MbCO) samples, the purified protein was dissolved in 99.8 % D_2O (Cambridge Isotope Laboratories) with (gel samples) or without (solution samples) a buffer. For ^{17}O MRD experiments, 20 % ^{17}O-enriched D_2O was used. By using D_2O for both ^{2}H and ^{17}O MRD experiments, correlation times can be compared directly without correcting for the (unknown) H/D kinetic isotope effect.

The solution was centrifuged at 13 000 rpm for 3 min to remove any insoluble protein, flushed by CO gas for 3 min on ice, and equilibrated by stirring for 30 min at 6 °C. Mb was then reduced by adding $\sim$ 2 equivalents of sodium dithionite (Sigma) and the process of flushing CO gas for 2 – 3 min and stirring for 30 min was repeated

(usually five times) until no further change in the optical absorption spectrum[63] (350 – 650 nm) could be detected (Shimadzu UV-1800). The Mb concentration was determined from the absorbance at 542 nm with an extinction coefficient, 18.4 mM^{-1} cm^{-1}, that had been calibrated using complete amino acid analysis (performed at Amino Acid Analysis Center, Dept. of Biochemistry and Organic Chemistry, Uppsala University, Sweden). MRD measurements were performed on seven solution samples with 2.0 – 2.6 mM Mb and on 26 gel samples, 23 of them with 1.6 – 1.7 mM Mb (Table S1).

The protein was immobilized by adding 25 % GA solution (Sigma) to the MbCO solution at 6 °C.[64] Except for two cases (Table S1), the GA/Mb mole ratio, N_{GA}, was in the range 29.7 – 31.1. After mixing by pipetting, an aliquot ($\sim$ 50 µl) of the solution was removed for pH measurement and the remainder was transferred to a glass tube (8 mm o.d. × 12 mm height), where it was cross-linked overnight at 6 °C. For the solution samples, pH was adjusted by adding either HCl or NaOH. Reported pD values are corrected for the H/D isotope effect according to pD = pH^* + 0.41, where pH^* is the reading on a pH meter calibrated with H_2O buffers.[65]

To pressurize Xe in a cross-linked MbCO sample, the protein was immobilized in a 10-mm heavy wall NMR tube with a pressure/vacuum valve (Wilmad). After cross-linking, the NMR tube was filled with 8 bar Xe gas (AGA, Sweden) and equilibrated for one week before NMR experiments. To estimate the Xe concentration in the MbCO sample, two reference samples (cyclohexane and 50 mM PIPES pD 7.4 in D_2O) were prepared. The reference solutions were placed in standard 10-mm NMR tubes and Xe gas was bubbled through the liquid.

2.2. NMR experiments

The water ^{2}H or ^{17}O longitudinal relaxation rate, R_1, was recorded on six different NMR set-ups: (1) a Stelar Spinmaster 1 T fast field-cycling (FC) spectrometer (^{2}H: 1.5 kHz – 5.4 MHz); (2) a Tecmag Apollo console equipped with a GMW field-variable ($\leq$ 1.8 T) iron-core magnet (^{17}O: 0.7 – 1.6 MHz); (3) a Tecmag Discovery console equipped with a Drusch field-variable ($\leq$ 2.1 T) iron-core magnet (^{2}H: 2.5 – 13.1 MHz; ^{17}O: 2.2 – 11.5 MHz) or (4) with a Bruker 4.7 T superconducting magnet (^{2}H: 30.7 MHz; ^{17}O: 27.1 MHz); and (5) Varian DirectDrive 500 (^{17}O: 67.8 MHz) and (6) 600 (^{2}H: 92.1 MHz; ^{17}O: 81.3 MHz) spectrometers. For the ^{2}H FC measurements, pre-polarized single-pulse ($\leq$ 2.6 MHz) or inversion recovery ($>$ 2.6 MHz) sequences were used with pre-polarization and detection at 5.4 and 4.8 MHz, respectively.[66] On other spectrometers, the standard inversion recovery pulse sequences were used. ^{129}Xe spectra were recorded on a Varian DirectDrive 600 (^{129}Xe: 166 MHz) using a single 90° pulse. All NMR experiments were performed at 25.0±0.1 °C, maintained by a thermostated air flow. The sample temperature was checked with a thermocouple referenced to an ice–water bath and by recording the bulk solvent relaxation rate on a reference water or buffer sample.

2.3. Analysis of MRD data

Water ^{2}H and ^{17}O MRD profiles, $R_1(\omega_0)$, from *free-tumbling* Mb in *solution* samples were analyzed with the standard multi-component exchange model,[59,60]

$$R_1(\omega_0) = R_1^0 + \frac{1}{N_{\text{W}}}\left[N_{\text{H}}(\xi_{\text{H}} - 1)R_1^0 + \sum_k N_k R_1^k(\omega_0)\right], \quad (1)$$

where ω_0 is the Larmor frequency in rad s^{-1}, R_1^0 is the known (frequency-independent) bulk solvent relaxation rate and N_{W} is the known water/Mb mole ratio in the sample. The inverse proportionality of the excess relaxation rate, $R_1^{\text{ex}}(\omega_0) \equiv R_1(\omega_0) - R_1^0$, and N_{W} was used to normalize all MRD data to the same Mb concentration, corresponding to $N_{\text{W}} = 3 \times 10^4$. In Eq. (1), a component k, as identified by MRD profile analysis, may include several sites with similar correlation times (see below).

The first, frequency-independent, term within brackets in Eq. (1) refers to the external hydration shell, comprising N_{H} water molecules with average dynamic perturbation factor $\xi_{\text{H}} \equiv \tau_{\text{H}}/\tau_0$.[67] We estimate $N_{\text{H}} = 727$ by computing the solvent-accessible surface area for equine Mb (average of PDB structures 1DWR, 1WLA, and 2VIK) with a probe radius of 1.7 Å and dividing by the mean surface area, 10.75 Å^2, occupied by one water molecule.[67] The second term within brackets in Eq. (1) arises from internal water molecules (and labile deuterons), with N_k water molecules (or labile-deuteron water equivalents) in component k with intrinsic relaxation rate $R_1^k(\omega_0)$. Formally, N_k is the sum of occupancies of the sites belonging to component k. N_k can be non-integer since these sites may be partially occupied.

In MbCO, the iron is in the diamagnetic ferrous low-spin state so there is no paramagnetic contribution to the water ^{2}H or ^{17}O relaxation rate. The intrinsic relaxation rate, induced by the nuclear electric quadrupole coupling, is described in the model-free approach as[60,68]

$$R_1^k(\omega_0) = S_{\text{iso},k}^2 \omega_{\text{Q}}^2 \tau_{\text{C},k}\left[\frac{0.2}{1 + (\omega_0\tau_{\text{C},k})^2} + \frac{0.8}{1 + (2\omega_0\tau_{\text{C},k})^2}\right]. \quad (2)$$

The contribution from internal motions in the hydration site, typically on a sub-ps time scale, is negligibly small and has been omitted in Eq. (2). Here, $S_{\text{iso},k}$ is the usual isotropic orientational order parameter[59,60,68] and ω_{Q} is the rigid-lattice nuclear quadrupole frequency (8.70×10^5 rad s^{-1} for ^{2}H and 7.61×10^6 rad s^{-1} for ^{17}O).[59] The correlation time $\tau_{\text{C},k}$ is related to the tumbling time τ_{R} of

the protein (assumed to undergo spherical-top rotational diffusion) and the mean survival time (MST) $\tau_{S,k}$ of a water molecule in site k as[60,68] $1/\tau_{C,k} = 1/\tau_R + 1/\tau_{S,k}$. Note that the survival time, often referred to as the residence time in the literature, is the time interval from an arbitrary time point to the next water exchange event.[69]

The isotropic rank-2 rotational correlation time τ_R for Mb was obtained from molecular hydrodynamics calculations using the program[70] HYDROPRO v. 10 with the recommended[70,71] effective (non-hydrogen) atomic radius of 3.0 Å and the 1.45 Å resolution crystal structure 1DWR of equine MbCO.[7] Corrected to the viscosity of D_2O at 25 °C, we thus obtained $\tau_R = 11.1$ ns, close to the value, 11.9 ± 0.4 ns, deduced[72] (after correction to D_2O viscosity) from the field-dependent paramagnetic transverse relaxation rate of the proximal histidine $H^{\delta 1}$ in equine deoxy-Mb at 25 °C. Because of its oblate-like shape, Mb actually undergoes anisotropic rotational diffusion, but the computed 17 % span of the five asymmetric-top rotational correlation times cannot be resolved by our MRD data.

As it stands, Eq. (1) is strictly valid only in the fast-exchange regime, where the MST in each site k that contributes significantly to $R_1(\omega_0)$ is sufficiently short that $R_1^k(0)\tau_{S,k} \ll 1$. In the dilute regime, where $N_W \gg 1$, however, Eq. (1) remains valid to an excellent approximation for arbitrarily long MST, provided that N_k and $\tau_{C,k}$ in Eqs. (1) and (2) are reinterpreted as effective parameters according to[60,68]

$$\frac{N_k^{\text{eff}}}{N_k} = \frac{\tau_{C,k}^{\text{eff}}}{\tau_{C,k}} = \left[1 + \omega_Q^2 S_{\text{iso},k}^2 \tau_{C,k}\tau_{S,k}\right]^{-1/2} . \qquad (3)$$

Water ^{2}H MRD profiles from *immobilized* Mb in *gel* samples were analyzed with the exchange-mediated orientational randomization (EMOR) model,[62] which has recently been quantitatively validated with the aid of an ultra-long MD simulation of the protein BPTI.[69] Since the cross-linked protein cannot tumble, the water orientation is randomized by the exchange process itself, so that $\tau_{C,k} = \tau_{S,k}$. As a consequence, the conventional perturbation theory of spin relaxation is only valid in the fast-exchange regime, where $\omega_Q\tau_{S,k} \ll 1$. In this regime, the EMOR theory reduces to Eqs. (1) and (2) (with $\tau_{C,k} = \tau_{S,k}$). Outside this regime, meaning $\tau_{S,k} > 1/\omega_Q \approx 1$ µs, the general form of the EMOR theory, based on the stochastic Liouville equation, must be used.[62] All fits to ^{2}H MRD data from immobilized MbCO reported here are based on Eq. (4.7) of Ref. 62, which is exact in the dilute regime ($N_W \gg 1$). Whereas, in the solution case, each component k is modeled by the two parameters $N_k S_{\text{iso},k}^2$ and $\tau_{C,k}$ (or their effective counterparts), there are four parameters in the gel case: N_k, S_k, η_k, and $\tau_{S,k}$.[62] Two of these parameters are related to the isotropic order parameter as[62] $S_{\text{iso},k} = S_k(1 + \eta_k^2/3)^{1/2}$.

Since the ^{17}O nuclide has spin quantum number $I = 5/2$, the relaxation behavior is in general more complex than for ^{2}H with $I = 1$.[59,61] In the dilute regime, however, Eqs. (1) – (3) remain valid to an excellent approximation in the solution case.[59,73] In the gel case, approximate expressions[61] are available for arbitrary $\tau_{S,k}$, while for $\tau_{S,k} < 1/\omega_Q \approx 100$ ns the EMOR theory reduces to Eqs. (1) and (2), which are valid also for ^{17}O.[59,73]

In fitting these models to the MRD data we used the trust-region reflective nonlinear optimization algorithm[74] with uniform 0.5 % (^{17}O solution MRD) or 1.0 % (all other MRD profiles) R_1 error, estimated from the scatter of the frequency independent bulk relaxation rate, R_1^0. With this algorithm, the model parameters can be constrained to their physically admissible ranges.

3. Results and discussion

3.1. Overview of MRD

Because ^{2}H relaxation is relatively slow, the field-cycling technique[59,66] can be used to measure the MRD profile from immobilized Mb down to 1.5 kHz, allowing internal-water exchange to be monitored on time scales up to 10 µs. The drawback is that ^{2}H relaxation does not probe water deuterons exclusively, but also may contain a contribution from labile deuterons (LDs) in acidic protein side-chains.[59,61,75,76] (This problem is even more severe for ^{1}H MRD.[59,77,78]) An essential step in the interpretation of ^{2}H MRD data is therefore to separate the contributions from D_2O molecules and LDs. To do this, we use four strategies: (1) we vary pD to change the acid- and base-catalyzed LD exchange rate and to titrate the LD-bearing side-chains; (2) we use different buffers to examine buffer-catalyzed LD exchange; (3) we compare ^{2}H MRD profiles from immobilized Mb with profiles from solutions of free-tumbling Mb, where the LD effect is usually more pronounced; and (4) we record ^{17}O MRD profiles (for both immobilized and free-tumbling Mb), which monitor water molecules exclusively, but do not extend below 0.7 MHz.

In Secs. 3.2 – 3.4, we analyze the ^{2}H and ^{17}O MRD data. The interpretation of the data gives a consistent picture of the internal hydration of Mb, but involves several technical details. As a guide to the reader, we summarize the key findings here.

^{2}H MRD profiles from immobilized MbCO show three dispersion components with characteristic mean survival times (MSTs) of 5.6 µs, 121 ns, and 6 ns, respectively. The one with the slowest MST (5.6 µs) is the dominant component and is attributed to internal water molecules and labile ^{2}H in histidine side-

chains. The other two components are assigned to internal motions of His side-chains (121 ns) and to confined external water molecules (6 ns) as seen in the previous protein gel MRD study.[61] The pD dependence of the gel ^{2}H MRD profiles demonstrates that 5.2 ± 0.6 internal water molecules and two or three His side-chains are responsible for the 5.6 μs component.

Solution ^{2}H MRD profiles from free-tumbling MbCO can be described by a single dispersion component. This component is attributed to the two slow components (5.6 μs and 121 ns) and the obtained parameters are consistent with the gel profiles.

An ^{17}O MRD profile from immobilized MbCO reveals an additional internal water molecule with an MST of 32 ns. This water molecule is not evident in the ^{2}H MRD data, presumably because 180° flips about the water dipole axis reduces the ^{2}H order parameter. A solution ^{17}O MRD profile is described by a single component just like the solution ^{2}H MRD. The solution ^{17}O MRD can be accounted for by the 5.6 μs and 32 ns components, whereas the solution ^{2}H dispersion is produced by the 5.6 μs and 121 ns components. The gel and solution ^{17}O MRD profiles indicate that 3.9 ± 0.6 internal water molecules are responsible for the 5.6 μs component, whereas the ^{2}H analysis yields 5.2 ± 0.6. Our final estimate of 4.5 ± 1.0 internal water molecules with an MST of 5.6 μs is the average of the ^{2}H and ^{17}O derived results.

3.2. ^{2}H MRD from immobilized MbCO

^{2}H MRD profiles from MbCO immobilized by cross-linking with GA, which reacts primarily with lysine side-chains,[64] were recorded at different Mb concentrations, GA/Mb mole ratios (N_{GA}), pD values, buffer conditions, and temperatures; in all 25 profiles (Table S1). Figure 2a shows a typical profile, measured at pD 7.0. The first thing to note is that the low-frequency dispersion has a large amplitude, ~ 3 times (after N_W normalization) that obtained from the protein BPTI with three contributing internal water molecules.[61] The dominant contribution to this large dispersion is a component with an MST of 5.6 ± 0.5 μs (Fig. 2a, Table 1). To reveal any LD contribution to this large dispersion, we recorded MRD profiles at different pD values in the range 5.66 – 7.15. pD values outside this range were excluded by heme dissociation[63] and concomitant Mb aggregation (lower pD) or by the GA cross-linking chemistry[64] (higher pD).

Figure 2b shows the pD dependence of the zero-frequency excess relaxation rate $R_1^{ex}(0) \equiv R_1(0) - R_1^0$, extrapolated from the R_1 data with the aid of the parameters derived from fits to 22 individual MRD

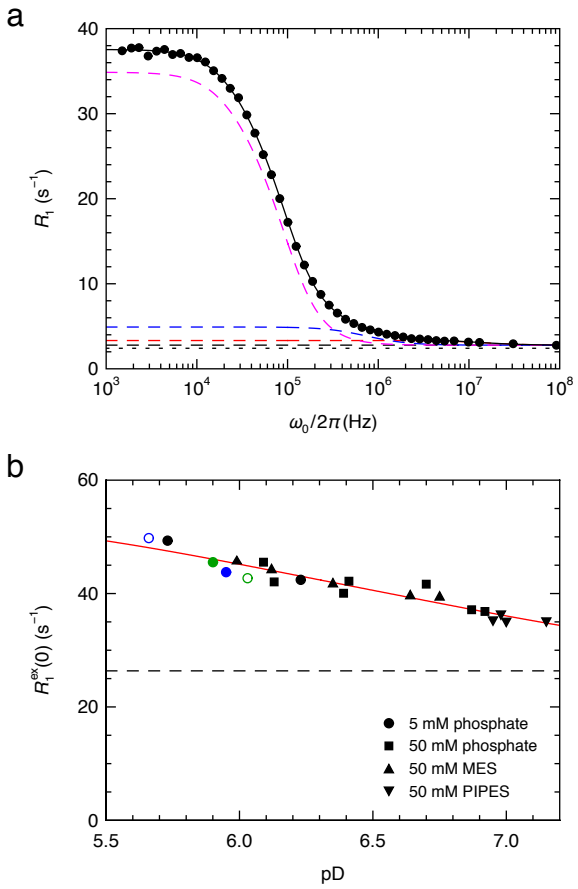


Figure 2. (**a**) ^{2}H MRD profile, $R_1(\omega_0)$, from immobilized MbCO at 25 °C, pD 7.0, and $N_{GA} = 29.9$, scaled to $N_W = 3 \times 10^4$. The error bars do not exceed the symbol size. The solid curve is the fit that resulted in the parameter values in Table 1. The dashed curves are dispersion components 1 (magenta), 2 (blue), and 3 (red). The bulk water (black dotted) and external hydration shell (black dashed) contributions are also shown. (**b**) Zero-frequency excess relaxation rate, $R_1^{ex}(0)$, obtained from fits to 22 MRD profiles, versus pD. The red curve is a fit based on the histidine pK_a values in Mb and the dashed line is the deduced pD-independent water contribution. The difference between the two curves hence represents the His LD contribution. Solid black symbols represent different buffer conditions as indicated. Colored symbols refer to different MbCO concentrations: 2.65 mM (green solid circle), 1.35 mM (green open circle), or 1.02 mM (blue solid circle); and N_{GA}: 110 (blue solid circle) or 62.1 (blue open circle). In all other cases, $C_{Mb} = 1.60$ – 1.67 mM and $N_{GA} = 29.7$ – 31.1.

Table 1. Results of fits to ^{2}H and ^{17}O MRD profiles.[a]

	immobilized Mb		free-tumbling Mb	
	^{2}H	^{17}O	^{2}H	^{17}O
$\tau_{C,1}$ (μs)	5.6 ± 0.5	[5.6]	–	–
N_1	6.7 ± 0.8	[5.2]	–	–
S_1	0.79 ± 0.02	[0.79]	–	–
η_1	0.3 ± 0.1	[0]	–	–
$\tau_{C,2}$ (ns)[b]	121 ± 10	32 ± 3	9.5 ± 0.5	5.6 ± 0.2
$N_2 S^2_{iso,2}$ [b]	0.70 ± 0.03	1.0 ± 0.1	5.6 ± 0.3	3.0 ± 0.1
$\tau_{C,3}$ (ns)	6.0 ± 1.0	4.3 ± 1.0	–	–
$N_3 S^2_{iso,3}$	3.6 ± 0.6	4.0 ± 0.6	–	–
ξ_H	7.3 ± 0.5	7.7 ± 0.4	5.7 ± 0.5	5.8 ± 0.1
χ^2_{red}	1.16	0.36	1.17	0.21

[a] All four MRD profiles were measured at 25 °C and pD 7.0. Quoted errors correspond to one standard deviation, propagated from the uniform 0.5 or 1.0 % uncertainty in R_1. Parameter values within square brackets were fixed during the fit.
[b] Component 2 has different physical origins in the four cases (see text).

profiles like the one in Fig. 2a (Table S1). Several conclusions can be drawn from these results. Since all data points fall on the same master curve despite having been recorded on samples with different Mb concentration (1.02 – 2.65 mM) and different N_{GA} (29.7 – 110), we infer that the internal-water dynamics probed by the MRD profile do not depend significantly on parameters that might affect the structure of the cross-linked protein network. When the Mb concentration was raised to 5.14 mM, however, a 23 % reduction of $R_1^{ex}(0)$ was observed. This might be due to impaired exchange for some of internal water molecules or labile deuterons caused by increased protein–protein contacts at high concentration. The subsequent analysis of MRD data from immobilized Mb is restricted to samples with $C_{Mb} \approx 1.6$ mM and $N_{GA} \approx 30$.

The second major conclusion that follows from the data in Fig. 2b is that $R_1^{ex}(0)$ must have a significant LD contribution. Before attempting to separate the pD-dependent LD contribution from the pD-independent internal-water contribution, we shall identify the side-chains and the exchange mechanism responsible for the LD contribution. In doing so we are guided by two observational facts: (1) the LD contribution to $R_1^{ex}(0)$ decreases with pD in the investigated pD range 5.66 – 7.15, and (2) the MST, τ_{LD}, of the LDs must be close to the 5.6 μs MST of the dominant dispersion component (Table 1). In the slow-exchange regime ($\tau_{LD} > 1$ μs), we expect the LD contribution to $R_1^{ex}(0)$ to be approximately proportional to $N_{LD}(pD)/\tau_{LD}(pD)$.[62] The observed pD dependence can hence reflect changes in the number, N_{LD}, of LDs and/or in τ_{LD}.

The LD exchange mechanism can be intermolecular (involving a single side-chain and one or more solvent species including buffer ions) or intramolecular (involving two proximal side-chains). We consider first the usual intermolecular mechanism. Due to the observed buffer independence of $R_1^{ex}(0)$ (Fig. 2b), buffer catalyzed LD exchange can be neglected. We therefore need to consider only the acid (D_3O^+) and base (OD^-) catalyzed exchange mechanisms. LD exchange from basic groups (Arg, Lys, His, N-terminus) is base catalyzed in the examined pD range. Any LD contribution from these groups would vary with pD as $N_{LD}/\tau_{LD} \propto 1/(10^{-pK_a} + 10^{-pD})$, that is, it would increase monotonically with pD, in contrast to the observed decrease (Fig. 2b). Furthermore, even if base catalyzed LD exchange proceeds at the maximum (diffusion controlled) rate, τ_{LD} at pD 7 is three orders of magnitude longer than the required μs time scale. LD exchange from hydroxyl-bearing groups (Ser, Thr, Tyr) is both acid and base catalyzed. In principle, the observed pD dependence (Fig. 2b) could therefore reflect acid catalysis. The rate constant, k_a, for acid catalysis is, however, typically four orders of magnitude smaller than the rate constant, k_b, for base catalysis.[75,76,79] The minimum LD exchange rate should therefore occur close to $pD^* = (1/2)\log[k_a/(K_W k_b)] \approx 5.5$, where $K_W = 10^{-14.95}$. In the examined pD range, we would therefore expect $R_1^{ex}(0)$ to increase with pD if hydroxyl LDs were responsible. Furthermore, even with the maximum conceivable rate constants[75,76,79] ($k_a \approx 10^7$ M^{-1} s^{-1} and $k_b \approx 10^{11}$ M^{-1} s^{-1}), τ_{LD} is too long, by at least two orders of magnitude, in the examined pD range. LD exchange from carboxyl groups (Asp, Glu, C-terminus) usually occurs directly to water without involvement of catalytic species, so that τ_{LD} is independent of pD.[75,76] In principle, the observed pD dependence (Fig. 2b) could therefore reflect deprotonation of COOD groups. For immobilized BPTI, a small COOD contribution was seen at pD 4.4, but not at pD 6.5 where all carboxyl groups in BPTI are deprotonated.[61] For MbCO, carboxyl groups with strongly upshifted pK_a are not indicated,[80] so carboxyl LDs cannot explain the pD dependence in Fig. 2b.

Based on these considerations, we conclude that the LD contribution observed here is produced by

intramolecular LD exchange with an essentially pD-independent rate. The observed pD dependence in $R_1^{ex}(0)$ must then reflect the ionization equilibrium. With no pK_a upshifted carboxyl group, only the imidazolium (His) groups are titrated in the examined pD range. Equine Mb contains 11 histidines (BPTI has none) with pK_a values in the neutral range (Table S2).[80–83] We then expect that $R_1^{ex}(0) = a + N_{LD}(pD)b$, where a is the internal water contribution and N_{LD} is the number of labile His deuterons (two in the acidic form, none in the basic form). Using published pK_a values,[80–83] we find that this function can reproduce the observed pD dependence in $R_1^{ex}(0)$. The fit shown in Fig. 2b yields a pD-independent contribution (the parameter a) to $R_1^{ex}(0)$ of 26.4 s^{-1}, corresponding to 73.1 % of $R_1^{ex}(0)$ at pD 7.0. Although all the His residues were included in this analysis, the result only depends on the pK_a distribution (in the examined pD range) and not on the number of His residues. Indeed, very similar results are obtained (26.2 s^{-1} and 73.3 %) if we assume that the pD dependence is produced by a single His residue with a typical pK_a value of 6.5.

The LDs of His side-chains can exchange via an intramolecular exchange mechanism, where a water molecule bridges a positive His residue and negative carboxylate group or a positive/neutral His pair (Sec. S1), similar to what has been proposed for certain low-molecular-weight His derivatives.[84] The crystal structure of equine MbCO reveals several His residues that could engage in such intramolecular exchange (Sec. S1, Fig. S1). A more detailed discussion of different exchange mechanisms for His LDs can be found in Sec. S1.

The ^{2}H MRD profiles from immobilized MbCO are strongly dominated by the slowest kinetic component (Fig. 2a), hereafter referred to as component 1. At pD 7.0, the fit yields $N_1 = 6.7 \pm 0.8$ for the number of water molecules and/or LD water equivalents (one acidic His residue equates to one D_2O molecule) responsible for this component (Table 1). Hydration sites may have fractional occupancy and His residues may be partly titrated, so N_1 need not be an integer. The analysis in Fig. 2b indicates that 73.1 % of $R_1^{ex}(0)$ is produced by water deuterons at pD 7.0 and the MRD fit in Fig. 2a shows that $R_1^{ex}(0)$ at pD 7.0 can be broken down as follows: 91.3 % component 1 (with contributions from water and LDs), 6.1 % component 2 (entirely due to LDs; see below), and 2.6 % from component 3 and the frequency-independent hydration-shell component (both entirely due to water; see below). We thus infer that $(73.1 - 2.6)/0.913 = 77.2$ % of component 1 is produced by $N_1^W = 0.772N_1 = 5.2 \pm 0.6$ internal water molecules.

The remaining 22.8 % of component 1 at pD 7.0 is attributed to LDs in His residues (see above). If the locally averaged nuclear quadrupole coupling is the same for the LDs as for the $\sim$ 5 internal water molecules, we can infer that $N_1^{LD} = 3.0 \pm 0.4$ LDs contribute to component 1 at pD 7.0. Since the (rigid-lattice) ^{2}H quadrupole coupling constant for the acidic imidazole deuterons[85] is expected to be smaller than for D_2O, the actual value of N_1^{LD} may be as large as five. We therefore conclude that at least two, and possibly three, His side-chains (with two LDs per imidazolium group) engage in water-mediated intramolecular LD exchange on the µs time scale.

According to the fit, the MST of the water molecules contributing to component 1 is $\tau_{S,1} = 5.6 \pm 0.5$ µs (Table 1). That $\sim$ 5 internal water molecules, located at different sites within the MbCO molecule, have the same MST suggests that they exchange by a common mechanism (Sec. 3.6). But it should be noted that even though the dominant low-frequency dispersion is reproduced by a single kinetic EMOR component, a modest MST distribution would not have been resolved by our data.

The value $\tau_{S,1} = 5.6$ µs is on the long side of the maximum of $R_1(0)$ versus τ_S, corresponding to $\tau_S \approx 1/\omega_Q \approx 1$ µs.[61,62] In this slow-exchange regime, $R_1(0)$ decreases with increasing τ_S. For example, if $\tau_{S,1}$ had been 1 µs, $R_1(0)$ would have been several-fold larger and the dispersion would have appeared at a higher frequency. If $\tau_{S,1}$ had been much longer, say 50 µs, then the dispersion frequency would only have been slightly downshifted, but the amplitude would have been strongly reduced.[62] In other words, a much larger number of internal water molecules or LDs would have been required to account for the observed MRD profile if the MST were much longer. In fact, in the ultraslow motion regime, where $\tau_S \gg 1/\omega_Q \approx 1$ µs, $R_1(\omega_0)$ is approximately proportional to N/τ_S.[62] Even though the observed 5.6 µs MST is not long enough to be in this regime, the parameters N_1 and $\tau_{S,1}$ have a sizeable covariance. Reassuringly, constrained fits to the ^{2}H MRD profile with different fixed values of N_1 yield the best fit quality for N_1 between six and seven (Fig. S2), consistent with the result, $N_1 = 6.7 \pm 0.8$, from the unconstrained fit.

To reproduce the ^{2}H MRD profile also at higher frequencies, the model must include, in addition to the dominant 5 μs component, two components in the fast-exchange regime (Table 1). One of these components has $\tau_{S,2} = 0.12 \pm 0.01$ μs and $N_2 S^2_{iso,2} = 0.70 \pm 0.03$. As argued in Sec. 3.4, this component can be attributed to internal motions of rapidly exchanging LDs in His side-chains. The third dispersion component has $\tau_{S,3} = 6 \pm 1$ ns and $N_3 S^2_{iso,3} = 3.6 \pm 0.6$ (Table 1). Similar parameter values were obtained for the highest-frequency component of the ^{2}H MRD profiles of immobilized BPTI and ubiquitin.[61] As before, we attribute this component to a small number of confined water molecules in the external hydration shell.[61] Finally, the dynamic perturbation factor, $\xi_H = 7.3 \pm 0.5$, deduced from the frequency-independent excess relaxation, is somewhat larger than for free-tumbling Mb (Sec. 3.3). This was also the case for immobilized BPTI ($\xi_H = 7.9 \pm 0.2$) and ubiquitin (6.0 ± 0.2),[61] both of which yield $\xi_H \approx 4$ for the free-tumbling proteins.[67] This difference between gel and solution samples, as well as the fact that component 3 is not observed in solution (Sec. 3.3 and 3.4), can be rationalized in terms of gel-induced confinement due to short intermolecular cross-links and/or intramolecular cross-links (equine Mb has 19 Lys residues).

In summary, the high-frequency tail of the ^{2}H MRD profile from immobilized MbCO exhibits the expected features associated with the external hydration shell, whereas the low-frequency part (components 1 and 2) reflects the occupancy and dynamics of internal hydration sites and LDs in a few His residues. The observed pD dependence of the ^{2}H MRD profile indicates that 5.2 ± 0.6 internal water molecules with MST 5.6 ± 0.5 μs contribute to the dominant dispersion component 1.

3.3. ^{2}H MRD from free-tumbling MbCO

As a check on the interpretation of the ^{2}H MRD data from immobilized MbCO, we measured the ^{2}H MRD profile from free-tumbling MbCO in solutions with pD in the range 5.0 – 10.0. (For the gel samples, the cross-linking chemistry[64] limited us to pD $\leq$ 7.2.) In the acidic pD range, a low-frequency MRD component was observed with a correlation time corresponding to tumbling of large protein aggregates, presumably induced by heme dissociation.[63] At pD 5.0, this component dominated the ^{2}H MRD profile. We therefore restrict the analysis to R_1 data measured at $\omega_0/2\pi > 0.9$ MHz on solutions with pD $\geq$ 6. Under these conditions, the fraction aggregated protein is so small ($\ll 1$ %) that the associated R_1 contribution can be neglected.

Figure 3a shows the ^{2}H MRD profile from free-tumbling MbCO at pD 7.0. At all pD values in the range 6.0 – 10.0, the MRD data (for $\omega_0/2\pi > 0.9$ MHz) can be adequately represented by a single dispersion component. The correlation time, τ_C, deduced from the single-component fit is shorter than the Mb tumbling time, $\tau_R = 11.1$ ns (Sec. 2.3) and it decreases with increasing pD: from 9.6 ± 0.4 ns at pD 6.0 to 7.4 ± 0.5 ns at pD 10.0 (Fig. 3b). These findings can be explained if there is a pD-dependent contribution from LDs exchanging on the ~ 100 μs time scale, as expected for base-catalyzed LD exchange in hydroxyl, ammonium, and guanidinium groups.[61,75,76,79] In contrast to the rapidly exchanging His LDs (Sec. 3.2), these more slowly exchanging LDs do not contribute to the ^{2}H MRD profile from immobilized MbCO because of the more restrictive fast-exchange criterion $\omega_Q \tau_S < 1$. For a free-tumbling protein, the fast-exchange criterion is $\omega_Q (\tau_R \tau_S)^{1/2} < 1$ (Sec. 2.3), so LDs with τ_S on the order of 100 μs make a significant contribution, albeit with reduced effective weight N^{eff} and correlation time τ_C^{eff} according to Eq. (3). As explained in more detail in Sec. S2, τ_C decreases with pD (Fig. 3b) because the relative contribution to the MRD profile from LDs with reduced effective correlation time increases with pD.

The pD dependence of the amplitude parameter $N S^2_{iso}$ has a broad minimum of 5.0 ± 0.3 at pD 8 – 9 (Fig. 3b). It decreases first because the His residues involved in intramolecular LD exchange are titrated (Sec. 3.2), consistent with the decrease of $R_1^{ex}(0)$ with pD in Fig. 2b. Above pD $\sim$ 9, where all His residues in equine Mb are titrated,[80–83] $N S^2_{iso}$ increases because base-catalyzed exchange brings an increasing number of hydroxyl-bearing or basic (mainly Arg) side-chains in Mb into the fast-exchange regime.[75]

The dynamic perturbation factor ξ_H for the external hydration shell does not vary significantly in the pD range 6.0 – 8.0, where $\xi_H = 5.5 \pm 0.2$ (mean $\pm$ standard deviation). This value is within the range found for other proteins.[67,86] At pD 10, $\xi_H = 6.5 \pm 0.6$ is slightly larger, most likely due to a frequency-independent R_1 contribution from sub-ns internal motions of rapidly exchanging LDs.[75]

The single component in the solution MRD profile (Fig. 3a) must include both components 1 and 2 in the gel MRD profile (Fig. 2a). In solution at pD 7.0,

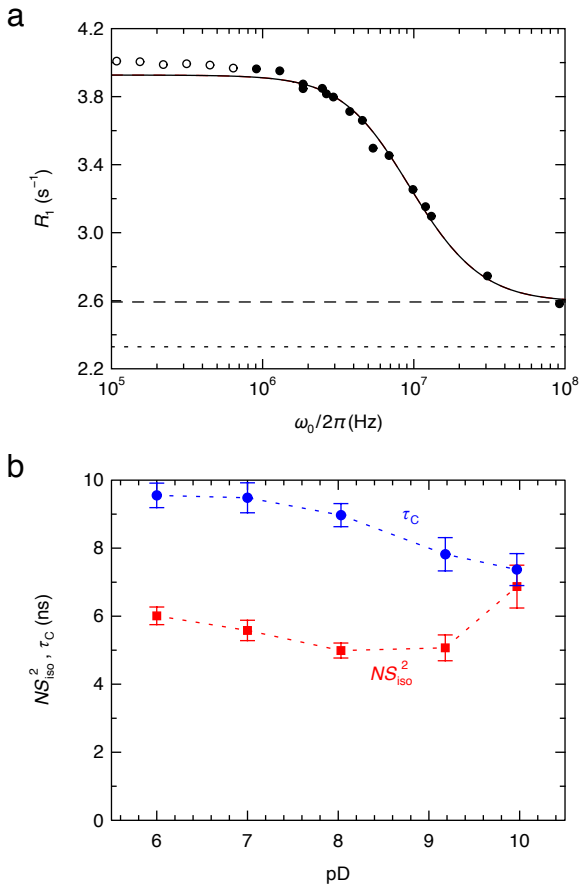


Figure 3. (**a**) ^{2}H MRD profile, $R_1(\omega_0)$, from free-tumbling MbCO at 25 °C and pD 7.0, scaled to $N_W = 3 \times 10^4$. The error bars are up to twice the symbol size. The solid curve is a single-component fit to the solid data points ($\omega_0/2\pi > 0.9$ MHz), with the parameters in Table 1. The bulk water (dotted line) and external hydration shell (dashed line) contributions are shown. (**b**) Amplitude NS^2_{iso} (red squares) and correlation time τ_C (blue circles), obtained from single-component fits to five MRD profiles, versus pD. The dotted lines are visual guides.

these two components should appear as a single (unresolved) component with amplitude (see Sec. 2.3) $NS^2_{iso} = N_1 S_1^2(1 + \eta_1^2/3) + N_2 S^2_{iso,2} = 5.0 \pm 0.9$ (Table 1), consistent with the value $NS^2_{iso} = 5.6 \pm 0.3$ deduced from the solution profile in Fig. 3a. A slightly different way of showing this consistency is to compute NS^2_{iso} as a function of N_1 using parameters from constrained gel MRD fits with different fixed N_1 values. The intersection of the resulting $NS^2_{iso} = f(N_1)$ curve with the solution value 5.6 ± 0.3 yields $N_1 = 7.2 \pm 0.6$ (Fig. S3). In this analysis, we ignored the minor contribution from slowly exchanging LDs to the solution NS^2_{iso} at pD 7.0. Using the minimum (at pD 8.0) solution value $NS^2_{iso} = 5.0 \pm 0.2$ we obtain instead $N_1 = 6.6 \pm 0.6$. In either case, the result of this analysis provides further support for the value $N_1 = 6.7 \pm 0.8$ obtained from the unconstrained fit (Table 1).

In summary, the mutually consistent ^{2}H MRD profiles from immobilized and free-tumbling protein indicate that MbCO contains 5.2 ± 0.6 highly ordered ($S = 0.79 \pm 0.02$) internal water molecules with a common MST of 5.6 ± 0.5 µs. In addition, the MRD profiles contain pD-dependent contributions from LD exchange and internal motions in His (neutral pD) and other (basic pD) side-chains.

3.4. ^{17}O MRD from immobilized and free-iumbling MbCO

While ^{17}O MRD is rigorously water selective, the fast ^{17}O relaxation precludes the use of field-cycling to access the low-frequency range of the 5 µs dispersion.[59] But even if this were possible, a water molecule with MST of 5 µs would be far into the slow-exchange regime (since ω_Q^2 is two orders of magnitude larger for ^{17}O than for ^{2}H) and it would therefore contribute very little to the ^{17}O MRD profile from immobilized MbCO.

Nevertheless, the ^{17}O MRD profile from *immobilized* MbCO at pD 7.0 exhibits a large dispersion in the examined frequency range (Fig. 4a). In analyzing this MRD profile, we include the small contribution from component 1, taking $\tau_{S,1} = 5.6$ µs and $S_1 = 0.79$ from the ^{2}H MRD fit (Table 1) and using the estimate $N_1 = 5.2$ for the number of water molecules associated with this component (Sec. 3.2). Even at the lowest frequency, this contribution hardly exceeds the measurement error in R_1 (Fig. 4a). Beyond this minor contribution, two fast-exchange components are required to account for the ^{17}O MRD profile (Table 1).

The dynamic perturbation factor ξ_H and the parameters $\tau_{S,3}$ and $N_3 S^2_{iso,3}$ of the fastest dispersion component do not differ significantly from the corresponding ^{2}H parameters (Table 1), as expected if these contributions reflect weakly anisotropic water motions in the external hydration shell in the gel. The amplitude parameter, $N^2_{iso,2} = 1.0 \pm 0.1$, of the slower ^{17}O component is similar to that of ^{2}H component 2 (Table 1), but the factor four difference in the associated correlation times shows that these components have different physical origins. A water molecule with 120 ns MST would give rise to a very

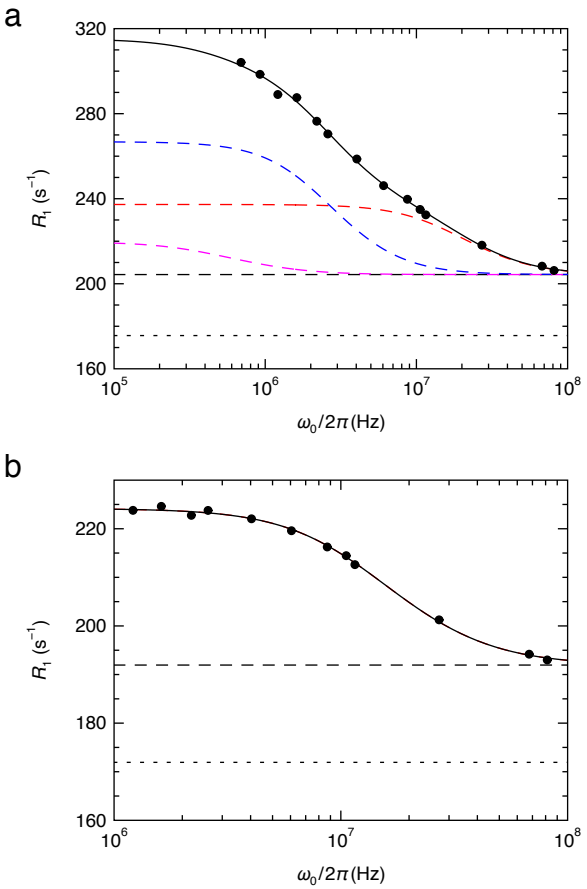


Figure 4. (**a**) ^{17}O MRD profile, $R_1(\omega_0)$, from MbCO gel at 25 °C, pD 7.0, and $N_{GA} = 29.9$, scaled to $N_W = 3{\times}10^4$. The error bars are up to twice the symbol size. The solid curve is the fit that resulted in the parameter values in Table 1. The dashed curves are dispersion components 1 (magenta), 2 (blue), and 3 (red). The bulk water (dotted line) and external hydration shell (dashed line) contributions are shown in both panels. (**b**) ^{17}O MRD profile, $R_1(\omega_0)$, from MbCO solution at 25 °C and pD 7.0, scaled to $N_W = 3 \times 10^4$. The error bars are comparable to the symbol size. The solid curve is a single-component fit, with the parameters in Table 1.

large ^{17}O dispersion, which is not observed, so we must conclude that this ^{2}H component is produced by LDs. Since 120 ns is too short to be an MST for a LD (all carboxyl groups are titrated at pD 7.0), we assign ^{2}H component 2 to internal motions of the His residues that contribute to ^{2}H component 1. Internal motions of protein side-chains on this time scale have previously been inferred from ^{2}H MRD studies of several proteins.[61,75,76]

^{17}O component 2, on the other hand, must reflect water motions. In principle, this could be local motions of the 5 μs internal waters. The only local water motion that might be as slow as 32 ns, however, is a 180° flip about the dipole axis, which, for symmetry reasons, cannot induce ^{17}O relaxation.[59] We therefore conclude that the dominant ^{17}O component 2 represents a single highly ordered water molecule with an MST of 32 ± 3 ns. This water molecule is unlikely to be deeply buried and it must exchange by a different mechanism than that used by the 5 μs waters. But why is this water molecule not evident as a 32 ns component in the ^{2}H profile? If it undergoes 180° flips on the time scale 0.1 – 10 μs, the ^{2}H parameter S^2_{iso} is reduced by a factor of three.[59] The contribution of this water molecule would then not be resolved because it would only add a small dispersion amplitude (0.3 s^{-1} in R_1) between the 6 ns and 121 ns dispersion steps (Fig. 2a).

As in the ^{2}H case, the ^{17}O MRD profile from *free-tumbling* MbCO is well described by a single dispersion component (Fig. 4b). The dynamic perturbation factor, $\xi_H = 5.8 \pm 0.1$, is the same as obtained from the ^{2}H solution profile (Table 1), as expected since water motions in the external hydration shell are nearly isotropic.[59] The correlation time, $\tau_C = 5.6 \pm 0.2$ ns, is shorter than the Mb tumbling time, $\tau_R = 11.1$ ns, because the single ^{17}O solution MRD component is an unresolved superposition of two components, both with correlation times shorter than τ_R. The first component, due to water molecules with $\tau_S = 5.6$ μs as deduced from the gel ^{2}H MRD profile, is in the intermediate-exchange regime for ^{17}O, with the effective correlation time shortened by a factor of ∼ 2 according to Eq. (3). The contribution of this component to the total amplitude parameter, $NS^2_{iso} = 3.0 \pm 0.1$ (Table 1), is reduced by the same factor. The second component, due to the single water molecule with $\tau_S = 32$ ns as deduced from the gel ^{17}O MRD profile, is in the fast-exchange regime with effective correlation time $(1/\tau_R + 1/\tau_S)^{-1} = 8.3 \pm 0.2$ ns (Sec. 2.3).

A quantitative analysis of the two contributions to $NS^2_{iso}\tau_C$, which is proportional to the magnitude of the dispersion, shows that the solution and gel ^{17}O MRD profiles are consistent, within the experimental error, with the gel ^{2}H MRD profile (Sec. S3, Fig. S4). Of particular interest is the number N_1^W of internal water molecules with an MST of 5.6 μs. Our analysis of the pD dependence of the gel ^{2}H MRD profile (Sec. 3.2) indicates that $N_1^W = 5.2$, but the ^{17}O MRD data suggest a somewhat smaller value (Sec. S3,

Fig. S4). Averaging these results, we arrive at the conservative estimate $N_1^W = 4.5 \pm 1.0$.

In summary, all the ^{2}H and ^{17}O MRD profiles measured on MbCO gels and solutions can be interpreted in a self-consistent way. The gel ^{2}H MRD profile and the solution ^{17}O MRD profile are both consistent with $N_1^W = 4.5 \pm 1.0$ ordered water molecules with an MST of 5.6 ± 0.5 μs. The solution and gel ^{17}O MRD profiles indicate an additional component, not resolved in the ^{2}H profiles, comprising a single highly ordered water molecule with an MST of 32 ± 3 ns.

3.5. Internal hydration sites

MRD experiments can provide the number of internal water molecules and their mean survival times, but the location of a hydration site can only be determined by MRD if the water molecule can be displaced by a ligand or a substituted side-chain.[59] Mb contains four cavities, denoted Xe1 – Xe4 (Fig. 1), that have been shown to bind xenon at elevated pressure.[52] To determine if the internal water molecules identified here occupy any of the Xe sites, we recorded the ^{2}H MRD profile from an MbCO gel that had been equilibrated with 8 bar Xe gas. We determined the Xe occupancies of these sites from ^{129}Xe NMR spectra of the MbCO gel and of two reference samples (Fig. S5), using also the reported[87] Xe binding constants for equine Mb at pH 7.0 and 25 °C. In this way, we obtained a Xe occupancy of 0.80 ± 0.09 for site Xe1 and a combined occupancy of 0.10 ± 0.05 for sites Xe2 – Xe4 (Sec. S4, Tables S3 and S4).

As seen from Fig. 5 and Table S5, Xe binding at this level has no significant effect on the ^{2}H MRD profile. With 80 % Xe occupancy in Xe1, we would have expected $100 \times 0.8/6.3 = 13$ % reduction of R_1 at low frequency if Xe1 had been fully occupied by a long-lived water molecule. We can therefore rule out internal water in this site. This is hardly surprising, since Xe1 has by far the highest Xe affinity[87] among the four Xe sites and thus is expected to be the least polar site. For the other sites, the combined 10 ± 5 % Xe occupancy is probably not sufficient to produce a detectable reduction of the MRD amplitude even if all these sites were fully occupied by water in the absence of Xe. If one Xe atom displaces one water molecule, MRD component 1 would be reduced by merely 1.5 % (0.1/6.7), comparable to the measurement error.

All high-resolution crystal structures of equine and sperm whale Mb, in the CO, deoxy, or met forms,[4–9] identify two internal hydration sites in the Xe3 cavity, with full (equine Mb) or nearly full (sperm whale Mb)

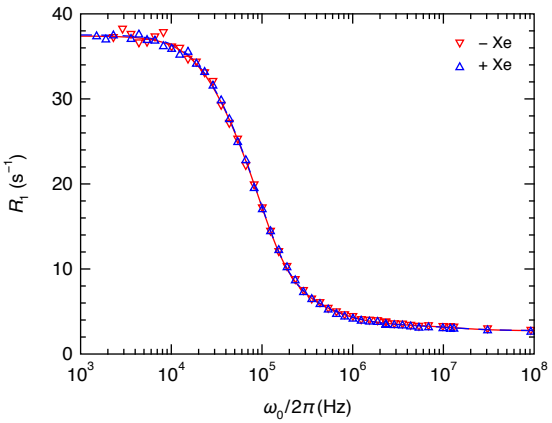


Figure 5. ^{2}H MRD profile, $R_1(\omega_0)$, from immobilized MbCO (25 °C, pD 7.16, scaled to $N_W = 3 \times 10^4$) in the presence (blue symbols) or absence (red symbols) of 8 bar xenon. The error bars do not exceed the symbol size. The parameter values obtained from the fits (solid red and dashed blue curves) are collected in Table S5.

occupancy (Figs. 1 and S6, Tables S6 and S7). The water molecule in subsite Xe3a has a small B factor and is engaged in four H-bonds, donating to Ile-75 O and His-82 $N^{\delta 1}$ and accepting from Gly-80 N and the adjacent water molecule. The water molecule in subsite Xe3b has a much larger B factor and makes only one H-bond with the protein (Ala-134 O). In addition, all but one of the high-resolution crystal structures listed in Tables S6 and S7 locate an internal water molecule in the so-called apical site (Figs. 1 and S6, Tables S6 and S7). The apical water makes three H-bonds with the protein. The crystal structures of equine Mb (but not sperm whale Mb) in the CO and deoxy (but not met) forms also locate a water molecule in the 'bottom' site (Figs. 1 and S6, Tables S6 and S7). The bottom water also makes three H-bonds with the protein, but it is less deeply buried than the apical water.

It is tempting to identify these four crystallographic water molecules with the 4.5 ± 1.0 most long-lived (5 μs) water molecules indicated by the MRD data. The Xe difference MRD experiment does not rule out the presence of two water molecules in the Xe3 cavity because Xe appears to displace only one of these water molecules (at least for sperm whale Mb; see PDB entries 1J52 and 2W6Y) and then, as noted above, the effect would be too small to detect. Furthermore, the 10 ± 5 % combined Xe occupancy is presumably associated mainly with the less polar Xe2 and Xe4 cavities. The 32 ns water inferred from

the ^{17}O MRD data might be located in a deep surface pocket. Alternatively, it could refer to one of the two least deeply buried among the four internal hydration sites, the bottom site and subsite Xe3b. In that case, another internal hydration site, not identified in the crystal structures, must contribute to the 5 μs MRD component. For example, the phantom (Ph) cavity (Fig. 1) is large enough to accommodate four (mutually H-bonded) water molecules, but this cavity is empty in all the crystal structures of equine Mb.

The two MD simulation studies that have focused on internal water in Mb both find multiple partially occupied hydration sites[44,51] most of which have not been identified in crystal structures. The first of these studies,[44] a conventional MD simulation of equine met-Mb at 300 K, found, in addition to the Fe^{3+}-bound water in the DP, eight internal hydration sites with a combined occupancy of 2.75. The apical site (occupancy 0.8) was identified, but not the bottom site. Both the Xe3 and Xe4 cavities were assigned an occupancy of 0.3. Except for the iron-bound water, all internal water molecules identified from this 48 ns MD trajectory exchanged on a nanosecond time scale. Therefore, this MD study supports neither the crystallographically inferred locations and occupancies of internal hydration sites in Mb nor the MRD-inferred microsecond time scale of internal water exchange.

The second simulation study[51] examined sperm whale deoxy-Mb at 310 K and used temperature-accelerated MD for enhanced sampling. Numerous internal hydration sites (but no occupancies) were reported, including the Xe2, Xe3, and Xe4 (but not Xe1) cavities. Based on computed minimum free energy pathways for water migration, it was suggested that all internal water molecules enter the protein via the His-64 gate and the DP, from where water molecules can migrate further to the Xe cavities. With the aid of transition state theory, the time scale for water escape from the DP was estimated to 300 ns (at 310 K), an order of magnitude faster than the 5 μs MST deduced from our MRD data.

In summary, crystallography[4–9] supports a scenario where most or all of the ∼ 4 long-lived internal water molecules inferred by MRD reside in small polar cavities (Xe3, apical, and bottom sites). A larger number of partially occupied sites, as suggested by MD simulations, is not likely to account for the MRD data. X-ray crystallography may miss hydration sites with low occupancy and/or positional disorder, but water molecules in less polar sites (say, with less than three H-bonds) are expected to have a small order parameter and would then not contribute much to the MRD profile.

3.6. Mechanism of internal-water exchange

The common MST, $\tau_S = 5.6 \pm 0.5$ μs, of the ∼ 4 water internal molecules inferred from our MRD data suggests that they exchange with external solvent via a common mechanism. Moreover, since the likely internal hydration sites are located far apart in the Mb molecule (the apical, bottom, and Xe3 sites are separated by 17, 27, and 31 Å), the common exchange mechanism must be global in spatial extent.

In an effort to gain more insight into the exchange mechanism, we studied the temperature dependence of the ^{2}H MRD profile from immobilized MbCO. Irreversible changes in the MRD profile, possibly caused by gel restructuring, were noted above 35 °C. Therefore, the analysis was restricted to the rather narrow temperature range 5 – 25 °C, where fits like the one in Fig. 2a yielded a surprisingly small Arrhenius activation energy of 17.4 ± 0.4 kJ mol^{-1} for the MST $\tau_{S,1}$ at pD 7.0 (Fig. S7). Such a small activation energy might suggest that water exchange is rate-limited by an entropic bottle-neck. The narrow temperature range and the strong covariance between N_1 and $\tau_{S,1}$ (Sec. 3.2), however, preclude an unambiguous interpretation of the temperature dependence. The MSTs used for the Arrhenius fit in Fig. S7 were obtained from constrained fits where $\tau_{S,1}$ was the only adjustable parameter for component 1 even though the relative contributions of internal water and LDs to component 1 are expected to vary with temperature.

The ∼ 5 μs MST deduced from our MRD analysis implies that internal-water exchange in Mb is a rare event that has not yet been captured by MD simulations, which so far do not extend beyond 100 ns for Mb. Neither the average protein structure seen in crystal structures nor the fluctuations accessed by sub-μs simulations tell us much about the transient structures involved in the water exchange event. An ultralong MD simulation[88] was recently used to demonstrate that the internal water molecules in the protein BPTI exchange by a transient aqueduct mechanism,[69] where single-file water chains penetrate the protein through transiently formed tunnels or pores. It is conceivable that a similar mechanism operates in Mb, with the difference that the transient water-filled tunnels are partly built from preexisting cavities. Whereas a single water molecule is unlikely to migrate from a polar site into a largely nonpolar cavity network,[55] an H-bonded water chain can move

rapidly through a transiently formed tunnel.[54] The peripherally located internal hydration sites might then act both as portals for solvent penetration and as seeds for transient water chains.

MD simulations indicate that the ligands can migrate from the DP into the extensive network of permanent and transient cavities that permeates the Mb molecule.[29,33,35,42,46] The ligand migration pathways seen in these simulations include the apical and Xe3 hydration sites.[32,35] A transient aqueduct mechanism might act to intermittently 'flush' the cavity network, thereby removing internally trapped ligands. Experiments[15,18,23,30,34,39] and simulations[35] indicate that photo-dissociated CO can escape from the DP via the His-64 gate on a 100 ns time scale. The half-life of CO that has migrated from the DP to the Xe1 cavity was, however, reported to be ~ 10 μs (at 20 °C).[19] Since this process occurs on the same time scale as internal-water exchange, it may, in fact, be concomitant with the proposed 'flushing' of the cavity system by transient water chains.

4. Conclusions

Based on ^{2}H and ^{17}O MRD measurements on gel and solution samples, we have arrived at the following answers to the first three of the five questions posed in Sec. 1:

(1) Under physiological conditions, equine MbCO contains 4.5 ± 1.0 internal water molecules that exchange on a μs time scale. The root-mean-square orientational order parameter of these water molecules is 0.8. Another ordered water molecule, possibly located in a deep surface pocket, exchanges on a time scale of 30 ns.

(2) The likely locations of the ~ 4 long-lived water molecules are the crystallographically identified Xe3, apical, and bottom hydration sites. In agreement with crystallography and MD simulations, the MRD results indicate that the Xe1 cavity is devoid of water.

(3) Despite being located as much as 30 Å apart, the ~ 4 long-lived internal water molecules have the same (or very similar) MST, $\tau_S = 5.6 \pm 0.5$ μs.

In addition, the MRD results indicate that two or three of the 11 His residues of equine Mb undergo intramolecular hydrogen exchange on a μs time scale.

As regards the last two questions in the Introduction, we speculate that

(4) The internal water molecules exchange by a global mechanism, that may involve penetration of the protein by transient H-bonded water chains, entering the protein at the peripherally located permanent hydration sites.

(5) The proposed water exchange mechanism suggests a functional role, where intermittent 'flushing' of the cavity system removes trapped ligands.

Acknowledgments

We thank Hanna Nilsson for help with sample purification. This work was financially supported by the Swedish Research Council. S.K. acknowledges postdoctoral fellowships from the Wenner-Gren Foundations and the Swedish Research Council.

References

1. J. B. Wittenberg and B. A. Wittenberg, *J. Exp. Biol.* **206**, 2011–2020 (2003).
2. U. Flögel, M. W. Merx, A. Gödecke, U. K. M. Decking, and J. Schrader, *Proc. Natl. Acad. Sci. U.S.A.* **98**, 735–740 (2001).
3. J. C. Kendrew, G. Bodo, H. M. Dintzis, R. G. Parrish, H. Wyckoff, and D. C. Phillips, *Nature* **181**, 662–666 (1958).
4. R. Maurus, C. M. Overall, R. Bogumil, Y. Luo, A. G. Mauk, M. Smith, and G. D. Brayer, *Biochim. Biophys. Acta* **1341**, 1–13 (1997).
5. G. S. Kachalova, A. N. Popov, and H. D. Bartunik, *Science* **284**, 473–476 (1999).
6. J. Vojtěchovský, K. Chu, J. Berendzen, R. M. Sweet, and I. Schlichting, *Biophys. J.* **77**, 2153–2174 (1999).
7. K. Chu, J. Vojtchovský, B. H. McMahon, R. M. Sweet, J. Berendzen, and I. Schlichting, *Nature* **403**, 921–923 (2000).
8. A. Ostermann, I. Tanaka, N. Engler, N. Niimura, and F. G. Parak, *Biophys. Chem.* **95**, 183–193 (2002).
9. H. P. Hersleth, T. Uchida, Å K. Røhr, T. Teschner, V. Schünemann, T. Kitagawa, A. X. Trautwein, C. H. Görbitz, and K. K. Andersson, *J. Biol. Chem.* **282**, 23372–23386 (2007).
10. R. H. Austin, K. W. Beeson, L. Eisenstein, H. Frauenfelder, and I. C. Gunsalus, *Biochemistry* **14**, 5355–5373 (1975).
11. H. Frauenfelder and P. G. Wolynes, *Science* **229**, 337–345 (1985).
12. S. M. Janes, G. A. Dalickas, W. A. Eaton, and R. M. Hochstrasser, *Biophys. J.* **54**, 545–549 (1988).
13. J. Smith, K. Kuczera, and M. Karplus, *Proc. Natl. Acad. Sci. U.S.A.* **87**, 1601–1605 (1990).
14. M. Lim, T. A. Jackson, and P. A. Anfinrud, *Science* **269**, 962–966 (1995).
15. J. S. Olson and G. N. Phillips Jr., *J. Biol. Chem.* **271**, 17593–17596 (1996).

16. M. Brunori, B. Vallone, F. Cutruzzolà, C. Travaglini-Allocatelli, J. Berendzen, K. Chu, R. M. Sweet, and I. Schlichting, *Proc. Natl. Acad. Sci. U.S.A.* **97**, 2058–2063 (2000).
17. W. Cao, J. F. Christian, P. M. Champion, F. Rosca, and J. T. Sage, *Biochemistry* **40**, 5728–5737 (2001).
18. E. E. Scott, Q. H. Gibson, and J. S. Olson, *J. Biol. Chem.* **276**, 5177–5188 (2001).
19. V. Šrajer, Z. Ren, T. Y. Teng, M. Schmidt, T. Ursby, D. Bourgeois, C. Pradervand, W. Schildkamp, M. Wulff, and K. Moffat, *Biochemistry* **40**, 13802–13815 (2001).
20. F. Schotte, M. Lim, T. A. Jackson, A. V. Smirnov, J. Soman, J. S. Olson, G. N. Phillips Jr., M. Wulff, and P. A. Anfinrud, *Science* **300**, 1944–1947 (2003).
21. N. Agmon, *Biophys. J.* **87**, 1537–1543 (2004).
22. G. Hummer, F. Schotte, and Anfinrud, P. A. *Proc. Natl. Acad. Sci. U.S.A.* **2004**, **101**, 15330–15334 (2004).
23. Y. Nishihara, M. Sakakura, Y. Kimura, and M. Terazima, *J. Am. Chem. Soc.* **126**, 11877–11888 (2004).
24. C. Tetreau, Y. Blouquit, E. Novikov, E. Quiniou, and D. Lavalette, *Biophys. J.* **66**, 435–447 (2004).
25. P. Banushkina and M. Meuwly, *J. Phys. Chem. B* **109**, 16911–16917 (2005).
26. C. Bossa, A. Amadei, I. Daidone, M. Anselmi, B. Vallone, M. Brunori, and A. Di Nola, *Biophys. J.* **89**, 465–474 (2005).
27. M. Schmidt, K. Nienhaus, R. Pahl, A. Krasselt, S. Anderson, F. Parak, G. U. Nienhaus, and V. Šrajer, *Proc. Natl. Acad. Sci. U.S.A.* **102**, 11704–11709 (2005).
28. S.-Y. Sheu, *J. Chem. Phys.* **122**, 104905 (2005).
29. J. Cohen, A. Arkhipov, R. Braun, and K. Schulten, *Biophys. J.* **91**, 1844–1857 (2006).
30. R. A. Goldbeck, S. Bhaskaran, C. Ortega, J. L. Mendoza, J. S. Olson, J. Soman, D. S. Kliger, and R. M. Esquerra, *Proc. Natl. Acad. Sci. U.S.A.* **103**, 1254–1259 (2006).
31. M. Anselmi, A. Di Nola, and A. Amadei, *Biophys. J.* **94**, 4277–4281 (2008).
32. M. Ceccarelli, R. Anedda, M. Casu, and P. Ruggerone, *Proteins* **71**, 1231–1236 (2008).
33. R. Elber and Q. H. Gibson, *J. Phys. Chem. B* **112**, 6147–6154 (2008).
34. R. M. Esquerra, R. A. Jensen, S. Bhaskaran, M. L. Pillsbury, J. L. Mendoza, B. W. Lintner, D. S. Kliger, and R. A. Goldbeck, *J. Biol. Chem.* **283**, 14165–14175 (2008).
35. J. Z. Ruscio, D. Kumar, M. Shukla, M. G. Prisant, T. M. Murali, and A. V. Onufriev, *Proc. Natl. Acad. Sci. U.S.A.* **105**, 9204–9209 (2008).
36. Y. Kiyota, R. Hiraoka, N. Yoshida, Y. Maruyama, T. Imai, and F. Hirata, *J. Am. Chem. Soc.* **131**, 3852–3853 (2009).
37. M. A. Scorciapino, A. Robertazzi, M. Casu, P. Ruggerone, and M. Ceccarelli, *J. Am. Chem. Soc.* **131**, 11825–11832 (2009).
38. A. Tomita, T. Sato, K. Ichiyanagi, S. Nozawa, H. Ichikawa, M. Chollet, F. Kawai, S.-Y. Park, T. Tsuduki, T. Yamato, S. Koshihara, and S. Adachi, *Proc. Natl. Acad. Sci. U.S.A.* **106**, 2612–2616 (2009).
39. H. S. Cho, N. Dashdorj, F. Schotte, T. Graber, R. Henning, and P. Anfinrud, *Proc. Natl. Acad. Sci. U.S.A.* **107**, 7281–7286 (2010).
40. R. Elber, *Curr. Opin. Struct. Biol.* **20**, 62–167 (2010).
41. R. M. Esquerra, I. López-Peña, P. Tipgunlakant, I. Birukou, R. L. Nguyen, J. Soma, J. S. Olson, D. S. Kliger, and R. A. Goldbeck, *Phys. Chem. Chem. Phys.* **12**, 10270–10278 (2010).
42. L. Maragliano, G. Cottone, G. Ciccotti, and E. Vanden-Eijnden, *J. Am. Chem. Soc.* **132**, 1010–1017 (2010).
43. Y. Nishihara, S. Kato, and S. Hayashi, *Biophys. J.* **98**, 1649–1657 (2010).
44. M. A. Scorciapino, A. Robertazzi, M. Casu, P. Ruggerone, and M. Ceccarelli, *J. Am. Chem. Soc.* **132**, 5156–5163 (2010).
45. M. Takayanagi, C. Iwahashi, and M. Nagaoka, *J. Phys. Chem. B* **114**, 12340–12348 (2010).
46. T.-L. Lin and G. Song, *Proteins* **79**, 2475–2490 (2011).
47. N. Plattner and M. Meuwly, *Biophys. J.* **102**, 333–341 (2012).
48. M. D. Salter, G. C. Blouin, J. Soman, E. W. Singleton, S. Dewilde, L. Moens, A. Pesce, M. Nardini, M. Bolognesi, and J. S. Olson, *J. Biol. Chem.* **287**, 33163–33178 (2012).
49. T. Tsuduki, A. Tomita, S. Koshihara, S. Adachi, and T. Yamato, *J. Chem. Phys.* **136**, 165101 (2012).
50. L. Boechi, M. Arrar, M. A. Martí, J. S. Olson, A. E. Roitberg, and D. A. Estrin, *J. Biol. Chem.* **288**, 6754–6762 (2013).
51. M. Lapelosa and C. F. Abrams, *J. Chem. Theory Comput.* **9**, 1265–1271 (2013).
52. R. F. Tilton Jr., I. D. Kuntz Jr., and G. A. Petsko, *Biochemistry* **23**, 2849–2857 (1984).
53. S. J. Hubbard and P. Argos, *Protein Eng.* **8**, 1011–1015 (1995).
54. J. C. Rasaiah, S. Garde, and G. Hummer, *Annu. Rev. Chem. Phys.* **59**, 713–740 (2008).
55. H. Yu and S. W. Rick, *J. Phys. Chem. B* **114**, 11552–11560 (2010).
56. S. Aime, P. Ascenzi, M. Fasano, and S. Paoletti, *Magn. Reson. Chem.* **31**, S85–S89 (1993).
57. T. E. Zewert, H. B. Gray, and I. Bertini, *J. Am. Chem. Soc.* **116**, 1169–1173 (1994).
58. V. P. Denisov and B. Halle, *Faraday Discuss.* **103**, 227–244 (1996).
59. B. Halle, V. P. Denisov, and K. Venu, in *Biological Magnetic Resonance*, Vol. 17, edited by N. R. Krishna and L. J. Berliner (Kluwer/Plenum, New York, 1999), pp. 419–484.
60. B. Halle, V. P. Denisov, K. Modig, and M. Davidovic, in *Protein Foldidng Handbook*, Vol. I, edited by J. Buchner and T. Kiefhaber (Wiley-VCH, Weinheim, Germany, 2005), Chap. 8, pp. 201–246.
61. E. Persson and B. Halle, *J. Am. Chem. Soc.* **130**, 1774–1787 (2008).
62. T. Nilsson and B. Halle, *J. Chem. Phys.* **137**, 54503 (2012).
63. E. Antonini and M. Brunori, *Hemoglobin and Myoglobin in their Reactions with Ligands* (North-Holland, Amsterdam, 1971).
64. I. Migneault, C. Dartiguenave, M. J. Bertrand, and K. C. Waldron, *Biotechniques* **37**, 790–802 (2004).
65. A. K. Covington, M. Paabo, R. A. Robinson, and R. G. Bates, *Anal. Chem.* **40**, 700–706 (1968).
66. G. Ferrante and S. Sykora, *Adv. Inorg. Chem.* **57**, 405–470 (2005).
67. C. Mattea, J. Qvist, and B. Halle, *Biophys. J.* **95**, 2951–2963 (2008).
68. B. Halle, *J. Chem. Phys.* **131**, 224507 (2009).
69. F. Persson and B. Halle, *J. Am. Chem. Soc.* **135**, 8735–

8748 (2013).
70. A. Ortega, D. Amorós, and J. García de la Torre, *Biophys. J.* **101**, 892–898 (2011).
71. B. Halle and M. Davidovic, *Proc. Natl. Acad. Sci. U.S.A.* **100**, 12135–12140 (2003).
72. D. Wang, U. Kreutzer, Y. Chung, and T. Jue, *Biophys. J.* **73**, 2764–2770 (1997).
73. B. Halle and H. Wennersröm, *J. Magn. Reson.* **44**, 89–100 (1981).
74. T. F. Coleman and Y. Li, *SIAM J. Optim.* **6**, 418–445 (1996).
75. V. P. Denisov and B. Halle, *J. Mol. Biol.* **245**, 698–709 (1995).
76. F. Vaca Chávez, E. Hellstrand, and B. Halle, *J. Phys. Chem. B* **110**, 21551–21559 (2006).
77. K. Venu, V. P. Denisov, and B. Halle, *J. Am. Chem. Soc.* **119**, 3122–3134 (1997).
78. F. Vaca Chávez and B. Halle, *Magn. Reson. Med.* **56**, 73–81 (2006).
79. E. Liepinsh and G. Otting, *Magn. Reson. Med.* **35**, 30–42 (1996).
80. D. Bashford, D. A. Case, C. Dalvit, L. Tennant, and P. E. Wright, *Biochemistry* **32**, 8045–8056 (1993).
81. S. Bhattacharya and J. T. J. Lecomte, *Biophys. J.* **73**, 3241–3256 (1997).
82. Y.-H. Kao, C. A. Fitch, S. Bhattacharya, C. J. Sarkisian, J. T. J. Lecomte, and B. García-Moreno E., *Biophys. J.* **79**, 1637–1654 (2000).
83. B. Rabenstein and E.-W. Knapp, *Biophys. J.* **80**, 1141–1150 (2001).
84. E. K. Ralph and J. N. Atherton, *J. Am. Chem. Soc.* **102**, 6184–6185 (1980).
85. X. Zhao and G. S. Harbison, *J. Phys. Chem. B* **110**, 25059–25065 (2006).
86. B. Halle, *Phil. Trans. R. Soc. Lond. B 359*, 1207–1224 (2004).
87. G. J. Ewing and S. Maestas, *J. Phys. Chem.* **74**, 2341–2344 (1970).
88. D. E. Shaw, P. Maragakis, K. Lindorff-Larsen, S. Piana, R. O. Dror, M. P. Eastwood, J. A. Bank, J. M. Jumper, J. K. Salmon, Y. Shan, and W. Wriggers, *Science* **330**, 341–346 (2010).
89. J. D. Müller, B. H. McMahon, E. Y. T. Chien, S. G. Sligar, and G. U. Nienhaus, *Biophys. J.* **77**, 1036–1051 (1999).
90. M. Eigen, *Angew. Chem. Int. Ed.* **3**, 1–19 (1964).
91. E. K. Ralph III and E. Grunwald, *J. Am. Chem. Soc.* **91**, 2422–2425 (1969).
92. E. Wilhelm, R. Battino, and R. J. Wilcoc, *Chem. Rev.* **77**, 219–262 (1977).
93. S. M. Rubin, M. M. Spence, B. M. Goodson, D. E. Wemmer, and A. Pines, *Proc. Natl. Acad. Sci. U.S.A.* **97**, 9472–9475 (2000).
94. G. L. Pollack, R. P. Kennan, J. F. Himm, and P. W. Carr, *J. Chem. Phys.* **90**, 6569–6579 (1989).
95. K. Oikarinen and J. Jokisaari, *Appl. Magn. Reson.* **8**, 587–595 (1995).
96. D. P. Hildebrand, D. L. Burk, R. Maurus, J. C. Ferrer, G. D. Brayer, and A. G. Mauk, *Biochemistry* **34**, 1997–2005 (1995).

Supporting information

Table S1. Samples for MRD experiments.

#	C_{Mb}[a]	type[b]	N_{GA}	pD	buffer[c]	nuclide	range (MHz)	n[d]
1	1.98	S		5.06		^{2}H	0.00152 – 92.1	34
2	2.43	S		6.00		^{2}H	0.00152 – 92.1	34
3	2.35	S		7.00		^{2}H	0.00152 – 92.1	34
4	2.38	S		8.03		^{2}H	0.00152 – 92.1	34
5	2.28	S		9.18		^{2}H	0.00152 – 92.1	34
6	2.22	S		9.97		^{2}H	0.00152 – 92.1	34
7	1.02	G	110	5.95	5 mM NaPi	^{2}H	0.00152 – 5.37	40
8	1.63	G	62.1	5.66	5 mM NaPi	^{2}H	0.00152 – 5.37	40
9	1.67	G	31.1	5.73	5 mM NaPi	^{2}H	0.00152 – 5.37	40
10	5.14	G	30.5	5.79	5 mM NaPi	^{2}H	0.00152 – 5.37	40
11	1.35	G	30.5	6.03	5 mM NaPi	^{2}H	0.00152 – 5.37	40
12	2.65	G	30.4	5.90	5 mM NaPi	^{2}H	0.00152 – 5.37	40
13	1.62	G	30.3	6.41	50 mM NaPi	^{2}H	0.00152 – 5.37	40
14	1.61	G	30.5	6.23	5 mM NaPi	^{2}H	0.00152 – 5.37	40
15	1.61	G	30.4	6.39	50 mM NaPi	^{2}H	0.00152 – 5.37	40
16	1.60	G	30.6	6.70	50 mM NaPi	^{2}H	0.00152 – 5.37	40
17	1.60	G	30.6	6.92	50 mM NaPi	^{2}H	0.00152 – 5.37	40
18	1.60	G	30.6	6.87	50 mM NaPi	^{2}H	0.00152 – 5.37	40
19	1.61	G	30.4	6.09	50 mM NaPi	^{2}H	0.00152 – 5.37	40
20	1.61	G	30.4	6.75	50 mM MES	^{2}H	0.00152 – 92.1	45
21	1.61	G	30.4	6.13	50 mM NaPi	^{2}H	0.00152 – 5.37	40
22	1.65	G	29.7	6.12	50 mM MES	^{2}H	0.00152 – 5.37	40
23	1.64	G	29.9	5.99	50 mM MES	^{2}H	0.00152 – 5.37	40
24	1.65	G	29.8	6.35	50 mM MES	^{2}H	0.00152 – 5.37	40
25[e]	1.65	G	29.8	6.64	50 mM MES	^{2}H	0.00152 – 5.37	40
26	1.61	G	30.4	6.75	50 mM MES	^{2}H	0.00152 – 92.1	45
27	1.62	G	29.9	6.98	50 mM PIPES	^{2}H	0.00152 – 5.37	40
28[e]	1.62	G	29.9	6.95	50 mM PIPES	^{2}H	0.00152 – 5.37	40
29	1.62	G	29.9	7.00	50 mM PIPES	^{2}H	0.00152 – 92.1	45
30	1.62	G	29.9	7.15	50 mM PIPES	^{2}H	0.00152 – 92.1	46
31[f]	1.62	G	29.9	7.17	50 mM PIPES	^{2}H	0.00152 – 92.1	46
32	2.57	S		7.03		^{17}O	1.21 – 81.3	12
33	1.62	G	29.9	7.02	50 mM PIPES	^{17}O	0.692 – 81.3	14

[a] MbCO concentration in mM. [b] Solution (S) or gel (G). [c] NaPi = sodium phosphate.
[d] Number of data points. [e] Measured at 5, 15, and 25 °C. [f] In presence of 8 bar Xe.

Table S2. pK_a^* values for titrating His residues in horse Mb.[a]

residue	pK_a^*		
	299.5 K, 0.2 M NaCl[81]	298 K, 20 mM NaCl[82]	298 K, 0.2 M NaCl[82]
36	7.75 ± 0.05	7.67 ± 0.01	7.80 ± 0.02
48	5.50 ± 0.07	5.42 ± 0.02	5.62 ± 0.01
81	6.86 ± 0.05	6.65 ± 0.01	6.94 ± 0.01
113	5.76 ± 0.07	5.51 ± 0.02	5.87 ± 0.02
116	6.72 ± 0.05	6.66 ± 0.02	6.79 ± 0.01
119	6.51 ± 0.05	6.38 ± 0.02	6.56 ± 0.01

[a] The number of labile His deuterons was calculated as $N_{\mathrm{LD}} = 2\sum_i [1 + 10^{\mathrm{pH}^* - \mathrm{p}K^*_{\mathrm{a},i}}]^{-1}$, where pH^* and $\mathrm{p}K^*_{\mathrm{a},i}$ are both measured in D_2O and neither are corrected for the H/D isotope effect (which largely cancels out in the difference). The set of six $\mathrm{p}K_a^*$ values used for the calculation in Sec. S1 were measured[82] at 298 K in 20 mM NaCl. In addition, we used $\mathrm{p}K_a^* = 5.91$ for His-97, determined for sperm whale MbCO.[89] The remaining four His residues are all in the basic from in the neutral pD range of interest here.[83,89]

S1. Histidine labile-deuteron exchange kinetics

We estimate the mean survival time, τ_{LD}, of the acidic imidazolium deuterons from

$$\tau_{\mathrm{LD}} = \frac{1}{k_{\mathrm{w}}[\mathrm{D_2O}] + k_{\mathrm{b}}[\mathrm{OD^-}] + k_{\mathrm{c}}\left[\mathrm{Buf^-}\right]} \ , \tag{S1}$$

where the three rate constants refer to the water, hydroxide, and buffer catalyzed exchange processes:

$$\begin{aligned} \geqslant\mathrm{ND^+} + \mathrm{D_2O} \quad &\xrightarrow{k_{\mathrm{w}}} \quad \geqslant\mathrm{N}: + \mathrm{D_3O^+} \\ \geqslant\mathrm{ND^+} + \mathrm{OD^-} \quad &\xrightarrow{k_{\mathrm{b}}} \quad \geqslant\mathrm{N}: + \mathrm{D_2O} \\ \geqslant\mathrm{ND^+} + \mathrm{Buf^-} \quad &\xrightarrow{k_{\mathrm{c}}} \quad \geqslant\mathrm{N}: + \mathrm{BufD} \ . \end{aligned}$$

Assuming that association and dissociation are diffusion-controlled with the rate constant k_{D}, the three LD exchange rate constants can be expressed as[90]

$$k = \frac{k_{\mathrm{D}}}{1 + 10^{\mathrm{p}K_{\mathrm{a}}(\mathrm{His}) - \mathrm{p}K_{\mathrm{a}}(\mathrm{BD})}} \ , \tag{S2}$$

where $\mathrm{p}K_{\mathrm{a}}(\mathrm{His})$ and $\mathrm{p}K_{\mathrm{a}}(\mathrm{BD})$ are the $\mathrm{p}K_{\mathrm{a}}$ of the acidic form of the His side-chain and of the conjugate acid BD of the base that accepts the deuteron from His, that is D_3O^+, D_2O, or BufD, respectively. For the following estimates, we ignore the H/D isotope effect, which largely cancels out in the $\mathrm{p}K_{\mathrm{a}}$ difference in Eq. (S2).

Taking $k_{\mathrm{D}} = 10^{10}$ M^{-1} s^{-1} (probably an overestimate), $\mathrm{p}K_{\mathrm{a}}(\mathrm{His}) = 6.38$ (the average of the values in the second $\mathrm{p}K_a^*$ column in Table S2), $\mathrm{p}K_{\mathrm{a}}(\mathrm{H_3O^+}) = -1.74$, and $sbr\mathrm{D_2O} = 55$ M, we obtain $k'_{\mathrm{w}} = k_{\mathrm{w}}[\mathrm{D_2O}] = 4.2 \times 10^3$ s^{-1} $\approx (240\ \mu\mathrm{s})^{-1}$. This estimate is close to the value, $k'_{\mathrm{w}} = 2.4 \times 10^3$ s^{-1}, measured by NMR for imidazole in H_2O at 25 °C.[91] For the hydroxide-catalyzed process, with $\mathrm{p}K_{\mathrm{a}}(\mathrm{H_2O}) = 15.74$, we obtain the estimate $k_{\mathrm{b}} = k_{\mathrm{D}} = 10^{10}$ M^{-1} s^{-1}. With $\mathrm{p}K_{\mathrm{a}}(\mathrm{D_2O}) = 14.95$ at 25 °C, we then obtain, at pD 7.0, $k_{\mathrm{b}}[\mathrm{OD^-}] = 10^{10} \times 10^{7.0-14.95}$ s^{-1} $\approx 1.1 \times 10^2$ s^{-1} $= (9\ \mathrm{ms})^{-1}$.

To make a significant contribution to the dominant component of the ^{2}H MRD profile (Fig. 2a), with a correlation time of ~ 5 µs, the mean survival time τ_{LD} of the labile His deuterons must also be ~ 5 µs. Our rough but conservative estimates show that the water and hydroxide catalyzed processes are too slow to contribute significantly. The buffer catalyzed process can also be ruled out, since a tenfold increase of the phosphate buffer concentration (from 5 to 50 mM) has no significant effect on $R_1(0)$ (Fig. 2b). Furthermore, at 50 mM buffer, no variation in $R_1(0)$ was observed between the phosphate ($\mathrm{p}K_{\mathrm{a}} = 7.20$), PIPES ($\mathrm{p}K_{\mathrm{a}} = 6.76$), and MES ($\mathrm{p}K_{\mathrm{a}} = 6.15$) buffers.

A remaining possibility is an internal catalysis such as $\geqslant \mathrm{ND}^{+}\cdots \mathrm{O_wD}\cdots {}^{-}\mathrm{OOC}$, where a water molecule connects the acidic His side-chain with a nearby proton acceptor, such as a carboxylate group or a basic His side-chain. The crystal structure[7] 1DWR of equine MbCO suggests several such possibilities (Fig. S1). For example, His-36 has an upshifted pK_a (Table S2),[81,82] presumably due to the proximity of Glu-38, the carboxylate group of which is bridged to His-36 via a H-bonding water molecule (Fig. S1a).

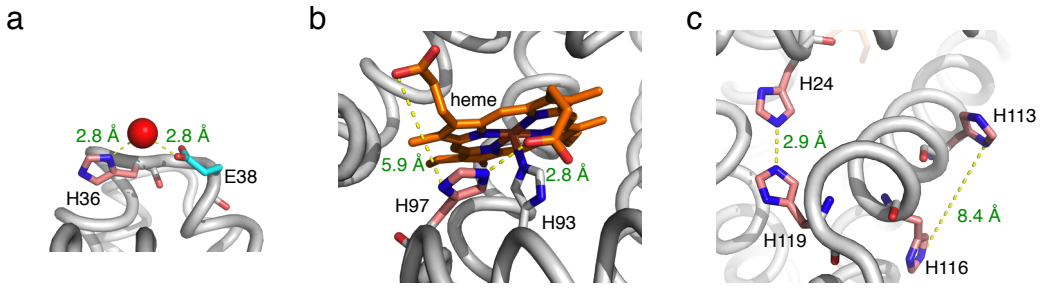


Figure S1. Possible internal catalysis of labile-deuteron exchange for (**a**) His-36, (**b**) His-97, and (**c**) His-24/His-119 and His-113/His-116. A red sphere represents a crystallographically identified water molecule.[7]

S2. pD-dependent effective correlation time

The overall correlation time, τ_C, deduced from one-component fits to solution ^{2}H MRD profiles (Fig. 3), decreases with pD even though $\tau_\mathrm{C}^\mathrm{eff}$ for the LDs increases with pD according to Eq. (3). This happens because LDs make a larger relative contribution to the MRD profile at higher pD. To understand this qualitatively, consider a single class of LDs with pD-dependent mean survival time $\tau_\mathrm{S}(\mathrm{pD})$. In view of Eq. (3), we then have approximately

$$\frac{\tau_\mathrm{C}}{\tau_\mathrm{R}} = \frac{N^\mathrm{W} + N^\mathrm{LD}/A}{N^\mathrm{W} + N^\mathrm{LD}/\sqrt{A}} \ , \tag{S3}$$

with

$$A = 1 + \omega_\mathrm{Q}^2 S_\mathrm{iso}^2 \tau_\mathrm{R} \tau_\mathrm{S}(\mathrm{pD}) \ . \tag{S4}$$

This heuristic expression predicts that $\tau_\mathrm{C} = \tau_\mathrm{R}$ at low pD, where τ_S is so long that the LD contribution is negligible compared to the internal-water contribution. With increasing pD, τ_S is shortened by base-catalyzed LD exchange. As a result, τ_C becomes progressively shorter than τ_R, as predicted by Eq. (S3). At still higher pD, τ_C exhibits a minimum and finally, when τ_S is so short that $A = 1$, τ_C again approaches τ_R. In practice, the minimum is not observed (at least not in our pD range) because new classes of LDs with smaller exchange rate constants gradually come into play as pD is increased.

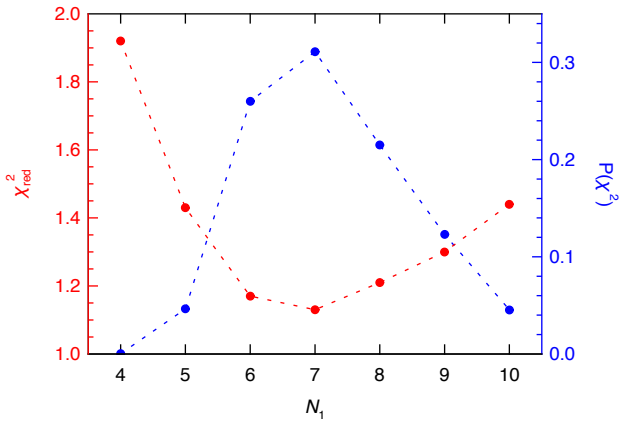


Figure S2. Reduced χ^2 and $P(\chi^2)$ for constrained fits to ^{2}H MRD profile from immobilized MbCO at pD 7.0 with N_1 for component 1 fixed in the fit.

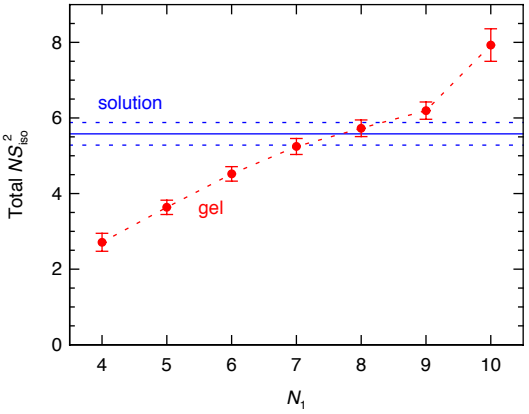


Figure S3. Amplitude parameter $NS^2_{\rm iso}$ from single-component fit to the solution ^{2}H MRD profile at pD 7.0 (blue line) and computed from the parameters of components 1 and 2 in constrained fits (fixed N_1) to the gel ^{2}H MRD profile at pD 7.0 (red circles).

S3. Mutual consistency of ^{2}H and ^{17}O MRD results

Here, we show that the parameters of the single component in the solution ^{17}O MRD profile is consistent with the results deduced from the gel ^{2}H and ^{17}O MRD profiles. To a good approximation, the product of the amplitude parameter and correlation time for the single ^{17}O solution MRD component can be expressed in terms of the parameters of the two components (identified in the gel MRD profiles) that it comprises:

$$NS^2_{\rm iso}\tau_{\rm C} = \frac{N_1^{\rm W} S^2_{{\rm iso},1}\tau_{\rm R}}{1+\omega_{\rm Q}^2 S^2_{{\rm iso},1}\tau_{\rm R}\tau_{{\rm S},1}} + N_2 S^2_{{\rm iso},2}\left[\frac{1}{\tau_{\rm R}}+\frac{1}{\tau_{{\rm S},2}}\right]^{-1}. \qquad \text{(S5)}$$

From the fit results in Table 1, we know that $NS^2_{\rm iso}\tau_{\rm C} = 16.8 \pm 0.8$ ns and that the second term on the right-hand side of Eq. (S5) equals 8.3 ± 0.8 ns. The two components thus make comparable contributions to the solution ^{17}O MRD profile. In the first term on the right-hand side of Eq. (S5), we know that $\omega_{\rm Q} = 7.61 \times 10^6$ rad s^{-1}, $\tau_{\rm R} = 11.1$ ns, and $\tau_{{\rm S},1} = 5.6$ µs (Table 1). In Eq. (S5), $S_{{\rm iso},1}$ refers to the ^{17}O order parameter, which may differ somewhat from the ^{2}H order parameter, $S_{{\rm iso},1} = S_1(1+\eta_1^2/3)^{1/2} = 0.80 \pm 0.02$

(Table 1). The ^{2}H order parameter pertains to internal water molecules as well as to rapidly exchanging LDs in a few His residues (Sec. 3.2).

From our analysis of the pD dependence of the gel ^{2}H MRD profiles, we estimated that component 1 comprises $N_1^{\mathrm{W}} = 5.2 \pm 0.6$ internal water molecules (Sec. 3.2). This result might be affected by modest systematic errors due to the strong covariance of N_1 and $\tau_{\mathrm{S},1}$ in the gel ^{2}H MRD fit and to inaccuracies in our analysis of the His LD contribution (Sec. 3.2). If our analysis of the gel ^{2}H and ^{17}O MRD profiles is quantitatively consistent, Eq. (S5) should be satisfied with $N_1^{\mathrm{W}} = 5.2$ and a reasonable ^{17}O order parameter $S_{\mathrm{iso},1}$. Figure S4 shows that Eq. (S5) is satisfied for ^{17}O $S_{\mathrm{iso},1}$ values from below 0.5 up to 0.83 when the propagated measurement errors are taken into account. Nonetheless, over most of this $S_{\mathrm{iso},1}$ range, Eq. (S5) predicts a smaller N_1^{W} value than the one deduced from the pD dependence of the gel ^{2}H MRD profiles. The ^{17}O order parameter is not likely to be substantially smaller than the ^{2}H order parameter. Assuming that $S_{\mathrm{iso},1} = 0.80$ also for ^{17}O, we obtain $N_1^{\mathrm{W}} = 3.9 \pm 0.6$ from Eq. (S5) (Fig. S4). Taking all available MRD data into account by averaging these two N_1^{W} values, we arrive at the more conservative estimate $N_1^{\mathrm{W}} = 4.5 \pm 1.0$.

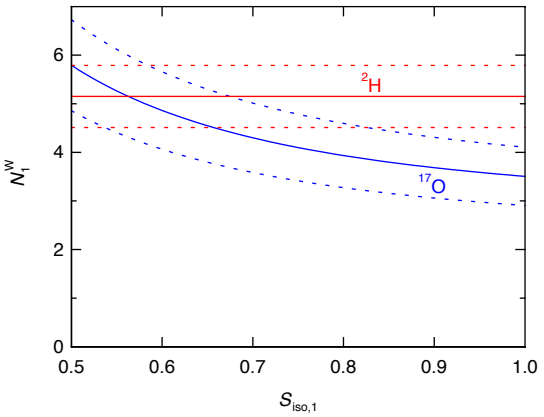


Figure S4. The number N_1^{W} of internal water molecules with MST 5.6 µs, deduced with the aid of Eq. (S5) from the solution and gel ^{17}O MRD profiles, as a function of the ^{17}O order parameter $S_{\mathrm{iso},1}$ (blue curve). Also shown is the N_1^{W} value obtained from the pD-dependent gel ^{2}H MRD profile (red line). The dotted curves or lines indicate the propagated measurement error.

S4. Determination of xenon occupancies

The Xe binding constants for equine Mb in the ferrous state at pH 7.0 and 25 °C have been reported as $K_1 = 94$ M^{-1} for the Xe1 site and $K_2 = 2.6$ M^{-1} for the weaker sites Xe2 – Xe4 (treated as one site).[87] We compute the Xe occupancy as

$$\theta_n = \frac{K_n[\mathrm{Xe}]}{1 + K_n[\mathrm{Xe}]} \ , \tag{S6}$$

where $n = 1$ or 2 and [Xe] is the free Xe concentration. We used ^{129}Xe NMR to determine the total Xe concentration $C_{\mathrm{Xe}} = [\mathrm{Xe}] + \theta C_{\mathrm{Mb}}$, where $\theta = \theta_1 + \theta_2$ and $C_{\mathrm{Mb}} = 1.62$ mM is the total MbCO concentration in the gel sample.

To determine C_{Xe} in the MbCO gel sample, we recorded ^{129}Xe NMR spectra (Fig. S5) from the gel equilibrated with 8 bar Xe (Sec. 2.1) and, for calibration purposes, from two reference samples (50 mM PIPES buffer in D_2O at pD 7.4 and cyclohexane) equilibrated with 1 atm Xe. The integrated intensity I_{Xe} of the Xe peak is proportional to the total Xe concentration C_{Xe} in the sample, but it also depends on the sample volume V (in the active region of the RF coil), the number N_{S} of accumulated scans (transients), the ^{129}Xe longitudinal relaxation rate R_1^{Xe}, and the recycle delay τ_{RD} according to

$$I_{\mathrm{Xe}} \propto C_{\mathrm{Xe}} V N_{\mathrm{S}} \left[1 - \exp\left(-R_1^{\mathrm{Xe}} \tau_{\mathrm{RD}}\right)\right] \ . \tag{S7}$$

The values of these parameters, along with the reported Xe concentration in the reference solvents (at 25 °C and 1 atm Xe) are collected in Table S3. The resulting total Xe concentrations C_{Xe} are given in Table S4, with errors propagated from the quoted intensity errors and an estimated 50 % uncertainty in R_1^{Xe} for the MbCO gel sample. The Xe occupancies θ_1 and θ_2 were then computed iteratively with the aid of Eq. (S6). In the main text, we use occupancies that are the averages of the values obtained with the two reference samples.

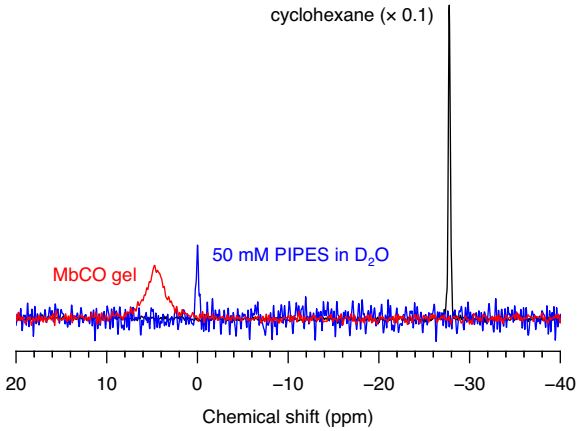


Figure S5. Natural abundance ^{129}Xe spectra recorded at 14.4 T and 25.0 °C from MbCO gel (8 bar Xe) and from the two reference samples, PIPES buffer and cyclohexane (1 atm Xe). The spectra are scaled to the same $N_{\mathrm{S}} = 256$ and, in addition, the spectrum from cyclohexane was multiplied by 0.1. The ^{129}Xe chemical shift scale is referenced to the PIPES buffer sample.

Table S3. Parameters used for determining Xe concentrations.

sample	I (a.u.)	C_{Xe} (mM)	V (µl)	N_{S}	τ_{RD} (s)	R_1^{Xe} (s^{-1})
MbCO gel	105.5 ± 1.1	–	530	2560	20.0264	0.033[a]
50 mM PIPES	1.678 ± 0.185	4.5[b]	720	256	300.0264	1.98×10^{-3} [c]
cyclohexane	33.77 ± 0.083	192[d]	710	128	60.0264	0.017[e]

[a] Estimated from ^{129}Xe spectra with different τ_{RD}. [b] Ref. 92. [c] Ref. 93. [d] Ref. 94. [e] Ref. 95.

Table S4. Xenon concentration and site occupancies in MbCO gel sample.

reference	C_{Xe} (mM)	occupancy, θ_n	
		Xe1	Xe2 – Xe4
50 mM PIPES	34.2 ± 13.2	0.76 ± 0.07	0.08 ± 0.03
cyclohexane	51.6 ± 18.8	0.83 ± 0.05	0.12 ± 0.04
average		0.80 ± 0.09	0.10 ± 0.05

Table S5. Results of fits to ^{2}H MRD profiles from immobilized MbCO at pD 7.2 and 25 °C with and without 8 bar Xe.[a]

parameter (unit)	−Xe	+Xe
$\tau_{C,1}$ (μs)	5.6 ± 0.8	[5.6]
N_1	[6.3]	6.32 ± 0.03
S_1	0.78 ± 0.02	[0.78]
η_1	0.4 ± 0.2	[0.4]
$\tau_{C,2}$ (ns)	127 ± 17	[127]
$N_2 S^2_{iso,2}$	0.69 ± 0.05	0.71 ± 0.2
$\tau_{C,3}$ (ns)	6.5 ± 1.3	[6.5]
$N_3 S^2_{iso,3}$	3.8 ± 0.8	3.6 ± 0.3
ξ_H	8.1 ± 0.8	8.3 ± 0.6
χ^2_{red}	3.15	2.38

[a] Due to slightly larger data scatter, a constrained fit was performed to the MRD profile in the absence of Xe, with $N_1 = 6.3$ fixed at the value expected from the pD 7.0 fit (Fig. 2a) and His pK_a values (Table S2). For the MRD profile in the presence of Xe, the unconstrained parameter values do not differ significantly from those obtained in the absence of Xe, demonstrating that the two data sets are indistinguishable within experimental error.

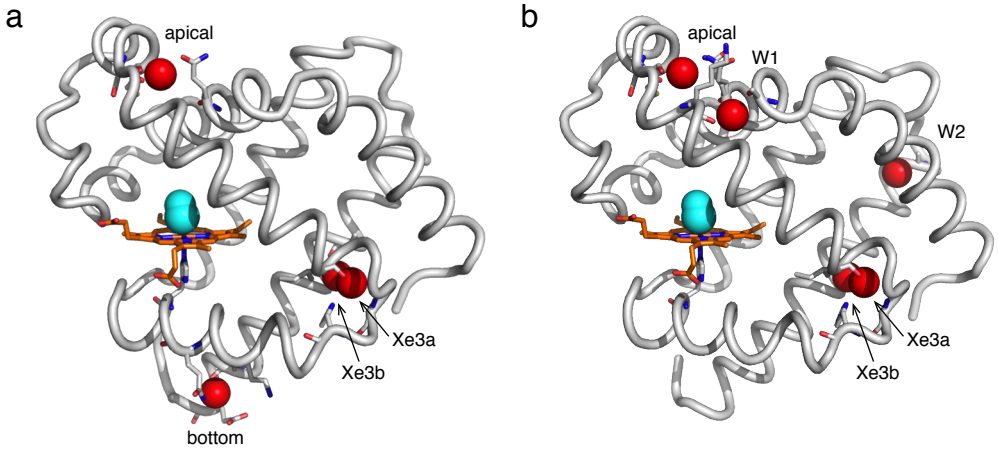


Figure S6. Internal water molecules (red spheres) in crystal structures of (**a**) equine MbCO (PDB: 1DWR[7]) and (**b**) sperm whale MbCO (PDB: 1A6G[6]) at cryogenic temperature.

Table S6. Internal water molecules in crystal structures of horse heart Mb.

PDB	form	res. (Å)	T (K)	pH	internal water characteristics			
					site (water no.)	occup.	B factor	H-bond acceptor/donor (length in Å)
1HRM[96]	H93Y, met?	1.70	n/a	n/a	Xe3a (160)	1.0	18.25	I75 O (2.9), G80 N (2.8), H82 $N^{\delta 1}$ (2.9), Xe3b (3.4)
					Xe3b (159)	1.0	34.00	A134 O (2.8), Xe3a (3.4)
1WLA[4]	met	1.70	n/a	n/a	DP (156)	1.0	8.26	Heme Fe, H64 $N^{\varepsilon 2}$
					Xe3a (180)	1.0	10.89	I75 O (2.9), G80 N (2.7), H82 $N^{\delta 1}$ (3.0), Xe3b (3.0)
					Xe3b (216)	1.0	38.98	A134 O (3.1), Xe3a (3.0)
					apical (217)	1.0	36.46	Q26 $N^{\varepsilon 2}$ (2.6), M55 O (2.7), S58 O (3.0)
1DWR[7]	CO	1.45	100	7.5	Xe3a (2072)	1.0	10.01	I75 O (2.9), G80 N (2.8), H82 $N^{\delta 1}$ (2.8), Xe3b (3.0)
					Xe3b (2106)	1.0	18.53	A134 O (3.0), Xe3a (3.0)
					apical (2059)	1.0	13.91	Q26 $O^{\varepsilon 2}$ (2.7), M55 O (2.8), S58 O (2.6)
					bottom (2078)	1.0	13.00	Q91 $N^{\varepsilon 2}$ (3.2), K145 O (3.0), E148 $O^{\varepsilon 2}$ (2.9)
2V1K[9]	deoxy	1.25	110	6.8	DP (2186)	1.0	32.80	Heme Fe (3.7), H64 $N^{\varepsilon 2}$ (3.6)
					Xe3a (2100)	1.0	14.13	I75 O (2.8), G80 N (2.9), H82 $N^{\delta 1}$ (2.8), Xe3b (3.0)
					Xe3b (2155)	1.0	20.92	A134 O (3.0), Xe3a (3.0)
					apical (2038)	1.0	20.87	Q26 $N^{\varepsilon 2}$ (2.6), M55 O (2.8), S58 O (2.7)
					bottom (2172)	1.0	16.89	Q91 $N^{\varepsilon 2}$ (2.9), K145 O (3.0), E148 $O^{\varepsilon 1}$ (2.6)

Table S7. Internal water molecules in crystal structures of sperm whale Mb.

PDB	form	res. (Å)	T (K)	pH	internal water characteristics			
					site (water no.)	occup.	B factor	H-bond acceptor/donor (length in Å)
1BZR[5]	CO	1.15	287	5.9	Xe3a (340)	1.0	18.25	I75 O (2.8), G80 N (2.9), H82 $N^{\delta 1}$ (2.8), Xe3b (3.1)
					Xe3b (403)	1.0	31.34	A134 O (3.1), Xe3a (3.1)
					apical (304)	0.65	18.07	Q26 $N^{\varepsilon 2}$ (2.9), M55 O (2.7), S58 O (2.7)
					W1 (382)	1.0	26.32	A22 O (2.7), K62 O (2.6)
1A6G[6]	CO	1.15	100	6.0	Xe3a (1006)	0.86	11.34	I75 O (2.8), G80 N (2.9), H82 $N^{\delta 1}$ (2.8), Xe3b (3.0)
					Xe3b (1056)	0.88	17.29	A134 O (2.9), Xe3a (3.0)
					apical (1053)	1.0	14.96	Q26 $N^{\varepsilon 2}$ (2.6–2.9), M55 O (2.9), S58 O (2.8)
					W1 (1011)	0.86	16.32	A22 O (2.6), K62 O (2.7)
					W2 (1154)	0.71	30.44	A127 O (2.7)
1BZ6[5]	met	1.20	287	6.0	DP (389)	1.0	8.86	Heme Fe (2.2), H64 $N^{\varepsilon 2}$ (2.7)
					Xe3a (352)	1.0	12.75	I75 O (2.8), G80 N (2.9), H82 $N^{\delta 1}$ (2.8), Xe3b (3.1)
					Xe3b (417)	1.0	34.98	A134 O (3.1), Xe3a (3.1)
					apical (509)	0.30	11.87	Q26 $O^{\varepsilon 1}$ (2.9), M55 O (2.8), S58 O (2.8)
					W1 (393)	1.0	19.83	A22 O (2.7), K62 O (2.7)
					W2 (500)	0.50	24.49	A127 O (3.0)
1A6K[6]	met	1.10	90	7.0	DP (1001)	1.0	9.70	Heme Fe (2.1), H64 $N^{\varepsilon 2}$ (2.7)
					Xe3a (1006)	0.93	10.64	I75 O (2.8), G80 N (2.8), H82 $N^{\delta 1}$ (2.7), Xe3b (3.0)
					Xe3b (1056)	0.83	14.77	A134 O (2.9), Xe3a (3.0)
					apical (1053)	1.0	11.55	Q26 $N^{\varepsilon 2}$ (2.6–3.0), M55 O (2.9), S58 O (2.8)
					W1 (1011)	0.93	13.02	A22 O (2.7), K62 O (2.7)
					W2 (1154)	0.70	23.42	A127 O (2.9)

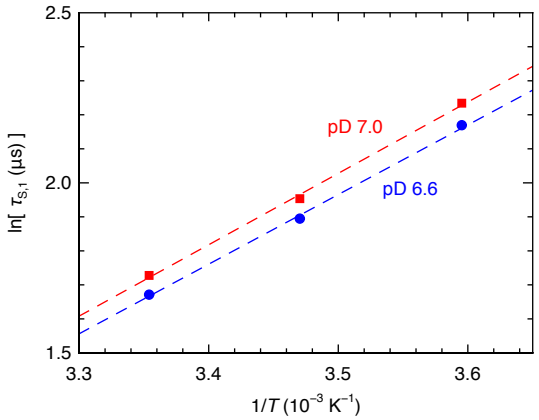


Figure S7. Arrhenius plot of the MST $\tau_{S,1}$ for component 1 in the ^{2}H MRD profile from immobilized MbCO at the indicated pD values. The slope yields $E_A = 17.4 \pm 0.4$ kJ mol^{-1} at pD 7.0 and 17.0 ± 0.3 kJ mol^{-1} at pD 6.6.